British Journal of Pharmacology

British Journal of Pharmacology (2016) **173** 2859–2879 2859

RESEARCH PAPER

Therapeutic potential of adipose stem cell-derived conditioned medium against pulmonary hypertension and lung fibrosis

Correspondence Dr Michael J. Katovich, Professor, Department of Pharmacodynamics, College of Pharmacy, University of Florida, Gainesville, Florida 32610, USA. Dr Vinayak Shenoy, Research Professor, Department of Pharmacodynamics, College of Pharmacy, University of Florida, Gainesville, Florida 32610, USA and Assistant Professor, Department of Pharmaceutical and Biomedical Sciences, California Health Sciences University, Clovis, California 93612, USA. E-mail: katovich@cop.ufl.edu; shenoyvi@cop.ufl.edu

Received 20 May 2015; **Revised** 7 July 2016; **Accepted** 10 July 2016

Anandharajan Rathinasabapathy[1,5], Erin Bruce[1], Andrew Espejo[1], Alana Horowitz[1], Dhivya R Sudhan[2], Anand Nair[3,6], Dominic Guzzo[1], Joseph Francis[3], Mohan K Raizada[4], Vinayak Shenoy[1,7] and Michael J Katovich[1]

[1]Pharmacodynamics, University of Florida, Gainesville, FL, USA, [2]Radiation Oncology, University of Florida, Gainesville, FL, USA, [3]Comparative Biomedical Sciences, Louisiana State University, Baton Rouge, LA, USA, [4]Physiology and Functional Genomics, University of Florida, Gainesville, FL, USA, [5]Allergy, Pulmonary and Critical Care Medicine, Vanderbilt University Medical Center, Nashville, TN, USA, [6]Pharmacology, University of Iowa, Iowa City, IA, USA, and [7]Pharmaceutical and Biomedical Sciences, California Health Sciences University, Clovis, CA, USA

BACKGROUND AND PURPOSE

Pulmonary hypertension (PH) and pulmonary fibrosis (PF) are life threatening cardiopulmonary diseases. Existing pharmacological interventions have failed to improve clinical outcomes or reduce disease-associated mortality. Emerging evidence suggests that stem cells offer an effective treatment approach against various pathological conditions. It has been proposed that their beneficial actions may be mediated via secretion of paracrine factors. Herein, we evaluated the therapeutic potential of conditioned media (CM) from adipose stem cells (ASCs) against experimental models of PH and PF.

EXPERIMENTAL APPROACH

Monocrotaline (MCT) or bleomycin (Bleo) was injected into male Sprague–Dawley rats to induce PH or PF respectively. A subset of MCT and Bleo animals were treated with ASCs or CM. Echocardiographic and haemodynamic measurements were performed at the end of the study. Lung and heart tissues were harvested for RNA, protein and histological measurements.

KEY RESULTS

CM treatment attenuated MCT-induced PH by improving pulmonary blood flow and inhibiting cardiac remodelling. Further, histological studies revealed that right ventricular fibrosis, pulmonary vessel wall thickness and pericyte distribution were significantly decreased by CM administration. Likewise, CM therapy arrested the progression of PF in the Bleo model by reducing collagen deposition. Elevated expression of markers associated with tissue remodelling and inflammation were significantly reduced in both PF and PH lungs. Similar results were obtained with ASCs administration.

CONCLUSIONS AND IMPLICATIONS

Our study indicates that CM treatment is as effective as ASCs in treating PH and PF. These beneficial effects of CM may provide an innovative approach to treat cardiopulmonary disorders.

Abbreviations

ASCs, adipose stem cells; A_T/E_T, acceleration time/ejection time; Bleo, bleomycin; BM-MSCs, bone marrow derived mesenchymal stem cells; CM, conditioned medium; ECHO, echocardiography; EPCs, endothelial progenitor cells; EDA, end diastolic area; EF, ejection fraction; LV, left ventricle; MCT, monocrotaline; PF, pulmonary fibrosis; PH, pulmonary hypertension; RV EDP, right ventricular end diastolic pressure; RVH, right ventricular hypertrophy; RVOT, right ventricular outflow tract; $RVOT_{Vmax}$, right ventricular outflow tract, maximum velocity; RVSP, right ventricular systolic pressure; SD, Sprague Dawley

DOI:10.1111/bph.13562

Tables of Links

TARGETS	
Other protein targets[a]	**Enzymes**[d]
TNFα	iNOS
GPCRs[b]	MMP12
CXCR4	
Catalytic receptors[c]	
TLR4	

LIGANDS		
CCL2	ICAM-1	MIP-1a (CCL3)
CINC-1 (CXCL1)	IL-1β	MIP-3a (CCL20)
CINC-2a (CXCL2)	IL-6	SDF-1 (CXCL12β)
CINC-2b (CXCL3)	IL-10	TGFβ
CTGF	IL-13	TIMP1
Dexamethasone	Indomethacin	VEGF
G-CSF	Insulin	
IBMX	LIX (CXCL5)	

These Tables list key protein targets and ligands in this article which are hyperlinked to corresponding entries in http://www.guidetopharmacology.org, the common portal for data from the IUPHAR/BPS Guide to PHARMACOLOGY (Southan *et al.*, 2016) and are permanently archived in the Concise Guide to PHARMACOLOGY 2015/16 ([a,b,c,d]Alexander *et al.*, 2015a,b,c,d).

Introduction

Pulmonary hypertension (PH) is a devastating, cardiopulmonary disorder that is associated with lung endothelial dysfunction, elevated pulmonary vascular resistance, and right ventricular overload, which eventually lead to heart failure and death (Schermuly *et al.*, 2011). Despite advances in our understanding of the disease pathology, and the availability of several pharmacological interventions (O'Callaghan *et al.*, 2011), there has been no significant improvement in patient survival or quality of life (Humbert *et al.*, 2010). Thus, this unmet medical condition necessitates the exploration of novel approaches for PH therapy. Similar to PH, idiopathic pulmonary fibrosis (IPF) is a fatal lung disease with poor prognosis, and median survival time of 3 years after diagnosis (Raghu *et al.*, 2011). However, unlike PH, IPF is associated with repetitive damage to the alveolar epithelial cells, which progressively results in tissue remodelling, extracellular matrix deposition and respiratory failure (Fernandez and Eickelberg, 2012). Treatment options for PF remain very limited and the management of IPF continues to pose significant challenges. Over the last decade, stem cell therapy has been gaining importance as a possible therapeutic strategy for treating numerous diseases including PH and PF (Anversa *et al.*, 2012).

Stem cells are self-renewing, multipotent undifferentiated cells, which can restore the function of injured tissue either by differentiating into various cell-types and/or by secreting paracrine factors. Stem cells isolated from the bone marrow (BM) include mononuclear, mesenchymal (BM-MSCs) and endothelial progenitor origin (EPCs), all of which have been investigated for their protective actions in experimental models of PH (Anversa *et al.*, 2012). Preliminary findings using EPCs suggested a therapeutic potential in combating PH; however, subsequent studies demonstrated that they provide only marginal benefit, and require genetic modification to enhance their therapeutic efficacy (Zhao *et al.*, 2005; Zhou *et al.*, 2013). Similarly, studies revealed modest effects with BM-MSCs in decreasing pulmonary pressure, suggesting that these cells may not be efficacious on their own, but can serve as a vector to deliver therapeutic genes (Takemiya *et al.*, 2010). In fact, some reports have shown that the recruitment of BM derived cells to the pulmonary vasculature may even aggravate the disease condition (Kanki-Horimoto *et al.*, 2006; Nikam *et al.*, 2010).

Adipose tissue has been identified as a repository of mesenchymal stem cells (MSCs), and these cells (ASCs - adipose stem cells) may be a better clinical-candidate (Kim and Heo, 2014). Isolation or maintenance of ASCs is minimally invasive and less laborious when compared with BM-MSCs or EPCs. Moreover, comparison of BM-MSCs and ASCs indicate that the latter may offer enhanced therapeutic benefits for treating certain pathological conditions (Ikegame *et al.*, 2011; Paul *et al.*, 2013). Recent reports have shown that cultured mesenchymal or stromal cells isolated from adipose tissue attenuate MCT-induced PH (Eguchi *et al.*, 2014; Somanna *et al.*, 2014; Luo *et al.*, 2015). Likewise, numerous preclinical studies have been conducted using various cell-types including alveolar epithelial type II cells (AECs), BM-MSCs and induced pluripotent stem cells (iPSCs) to treat Bleo-induced PF (McNulty and Janes, 2012). However, each of these interventions has uncovered some complicating issues. AECs were effective in preventing, attenuating or reversing the severity of PF (Serrano-Mollar *et al.*, 2007), but these cells can be obtained only from lung biopsies or during lung transplantation. In the case of BM cells, it was observed that fibrocytes associated with the BM-MSC population contributed to lung damage and fibrosis (Phillips *et al.*, 2004). With regards to iPSCs, genomic instability, clinical safety and ethical issues pose significant challenges (Okano *et al.*, 2013). In a recent study, ASCs were administered i.p. to treat a rodent model of PF; however, the effective route of administration is still debatable (Lee *et al.*, 2014). Thus, there are several limitations in using these stem cells.

It has been proposed that stem cells may exert their therapeutic benefits in a paracrine-like fashion rather than differentiating into specific cell-types (Salgado *et al.*, 2010). Paracrine mechanisms include the secretion of micro-vesicles/exosomes in addition to bioactive molecules (Salgado *et al.*,

2010; Sabin and Kikyo, 2014). To the best of our knowledge, no investigation has been reported assessing the beneficial effects of secretions of ASCs [conditioned medium (CM)] against PH or PF. Therefore, we hypothesized that the administration of CM alone could arrest the progression of PH or PF and attenuate the associated cardiopulmonary dysfunctions in both MCT and Bleo animal models of lung injury.

Methods

Animals

All animal procedures were approved by the Institutional Animal Care and Use Committee at the University of Florida and complied with the National Institutes of Health guidelines. All studies involving animals are reported in accordance with the ARRIVE guidelines for reporting experiments involving animals (Kilkenny *et al.*, 2010; McGrath and Lilley, 2015). The experimental protocols were carried out on 8 week old rats after a week acclimatization period within the animal care facility. Animals were housed in conventional cages with a 12:12 h light–dark cycle with free access to food and water. A total of 256 animals were used in the experiments described here.

Study design

Eight-week old male Sprague Dawley (SD) rats obtained from Charles River Laboratories, (Wilmington, MA, USA) were used in this study. A preliminary study was conducted to identify the best time to administer our therapeutic agents. PH was induced by a single injection (50 $mg \cdot kg^{-1}$, s.c.) of MCT (n = 12). Control animals were administered saline (n = 12). Every two weeks after the MCT challenge, the right ventricular systolic pressure (RVSP) measurement and echocardiographic assessment (ECHO) was performed on six animals from each group. In a subsequent study, 2 weeks after the MCT-insult, when the RVSP was significantly elevated, animals were administered eGFP-ASCs through a jugular catheter (MCT + A group, n = 8), to compare against the MCT group (n = 8). For this study, donor male rats [SD-Tg(UBC-eGFP)] ubiquitously overexpressing eGFP were purchased from RRRC (Columbio, MO, USA). Another group of animals were administered CM (MCT + CM, n = 8) after 14 days of MCT-insult and compared against a group of animals wherein, the same amount of concentrated plain media (no serum) was administered (MCT + M group, n = 8). Two weeks after the administration of ASCs or CM, RVSP measurement and ECHO assessment was performed. Animals were killed and tissues were harvested for RNA, protein, immunohistochemical (IHC) and immunofluorescence (IF) analysis. In order to validate the therapeutic benefits of ASCs or CM, we performed another similarly designed experiment (Control, MCT, MCT + M, MCT + DF, MCT + DF-CM, n = 7), wherein, we used dermal fibroblast (DF), plain media (M) and DF derived CM (DF-CM) in place of ASCs or ASCs-CM.

Similar to the PH experiments, we performed a preliminary study to evaluate the progression of fibrosis and tissue remodelling in PF. PF was induced by a single intratracheal injection (2.5 $U \cdot mL^{-1}$) of Bleo (n = 15). Control animals were administered saline (n = 15). After 3, 7 and 14 days of Bleo-instillation, RVSP was measured in 5 animals from each group. Animals were killed and lung tissue was processed for histological measurements. Based on the histological analysis, we decided to administer ASCs or CM after 3 (early phase) or 7 (late phase) days of Bleo-instillation; 8–9 week-old donor male SD rats (n = 5) were utilized to harvest the ASCs and prepare CM. For the early phase study (n = 8), ASCs (BAD3 group) or CM (BCM3 group) was administered through the jugular vein and compared against the B (Bleo) or B + M (Bleo + plain media) group respectively. In the late phase study (n = 8), ASCs (BAD7) or CM (BCM7) was administered after 7 days of Bleo-instillation and compared against B (Bleo) or B + M group respectively. A subsequent study was performed for the early and late phase treatments where whole lungs were collected to estimate the total lung collagen deposition. As it was a repeat study, n = 5 was maintained in each group. Since the ECHO, haemodynamic and histological parameters were identical for both the B and B + M groups in our previous experiments; we decided not to include the B + M group in this study. In both studies, similar terminal procedures were followed as described in the PH study. Rats were assigned randomly to different experimental groups for all *in vivo* studies. Two independent observers were blinded for data collection and evaluation of all *in vivo* and *in vitro* experiments.

Isolation of adipose stem cells

ASCs were isolated from 10–11 week-old male SD eGFP rat for the PH study and 8–9 week-old male rat for the PF study. In brief, the inguinal fat pad was minced and digested in 0.1% $w\ v^{-1}$ type 1 collagenase (Worthington Biochemical Corporation, Lakewood, NJ, USA) for 45 to 60 min, with intermittent shaking in a 37°C water bath. Subsequently, the digested cells were neutralized with FBS, passed through 100 μm cell-strainer, centrifuged and cultured in DMEM supplemented with 10% FBS and 1% antibiotic solution. After 6–8 h, unattached cells were removed by gentle washing and the attached cells were fed with fresh medium. Cells at passage 2–5 were used for all the experimental purpose. Cells were grown at 37°C incubator humidified with 5% CO_2.

Characterization of rat ASCs – flow cytometry

A total of 0.5×10^6 of cultured ASCs were incubated with CD44, CD90, CD34 and CD45 antibodies and analysed for their presence by FACSort flow cytometer (BD Pharmingen, San Jose, CA, USA). Flow data was analysed by BD FACSDIVA software, version 6.1.2 BD Biosciences, San Jose, CA, USA. Cells were also stained with the corresponding Isotype matched antibodies, IgG1 and IgG2A to measure the background fluorescence.

Characterization of rat ASCs – adipogenic, osteogenic and chondrogenic differentiation

In order to achieve adipocyte differentiation, confluent ASCs were incubated with a cocktail containing 200 μM indomethacin, 500 μM IBMX, 250 nM dexamethasone and 10 $\mu g \cdot mL^{-1}$ insulin. Following 6–9 days of incubation, ASCs were differentiated to mature oil-filled adipocytes. Adipocytes were stained with Oil Red 'O' and images were photographed. For osteocyte differentiation, confluent ASCs were incubated with the commercial osteogenesis cocktail (Life Technologies) as per the manufacturer's instructions. Differentiated osteocytes were stained with 2% Alizarin Red. For chondrocyte differentiation, 0.3×10^6 ASCs were incubated with the

commercial chondrogenesis cocktail (Life Technologies) as per the manufacturer's instructions in a 'U' bottom low attachment, 96-well plate (Corning). Differentiated osteocyte spheres were stained with Alcian Blue. Scale bar = 100 μm.

Preparation of conditioned medium (CM) from ASCs

A total of 1×10^6 of cultured ASCs in a 10 cm culture dish at passages 2–5 were washed three times in PBS to remove the FBS content and subsequently serum-starved for 24 h in 6 mL of plain DMEM medium. Post 24 h, this medium was collected, and centrifuged to remove any cell debris. Furthermore, this medium was concentrated to 100 μL using an Amicon Ultra-4 Centrifugal filter unit (EMD Millipore) with 3KDa cut-off, to obtain CM. Then 100 μL of CM (from 1×10^6 of ASCs) was administered to each animal in the respective CM groups through the jugular vein.

Characterization of ASCs-CM – rat cytokine array assay

In order to characterize the presence of cytokines in the CM, we used the Proteome Profiler Rat Cytokine Array Panel A Kit (R&D Systems, MN, USA). Instructions were followed as described in the kit.

Administration of ASCs or CM in MCT and Bleo-challenged rats

In the PH preliminary studies, we found that the mortality rate of animals was unacceptably high when we injected 3 or 5×10^6 ASCs as observed by others (Luo *et al.*, 2015). Therefore, for all subsequent studies, we scaled down the ASCs administration to 1×10^6 cells. Animals were anaesthetised under 2% isoflurane-oxygen mixture. The silastic cannula was inserted into right descending jugular vein and advanced to the right ventricle (RV). Then 1×10^6 of eGFP-ASCs in 100 μL of PBS was administered through the jugular vein in the MCT + A group. To evaluate the possible paracrine effects of ASCs, additional groups (MCT + CM) were utilized, where, 100 μL of CM, conditioned from 1×10^6 serum starved ASCs was administered in a similar manner. A total of 6 mL of plain culture medium without serum was concentrated to 100 μL and administered in a separate group (MCT + M), which served as a control for CM. After 2 weeks of ASCs or CM administration, animals were subjected to echocardiographic and haemodynamic measurements. For the early or late phase PF study, either ASCs or CM were injected after 3 or 7 days of Bleo-instillation through the jugular vein, and all other experimental procedures were followed as explained earlier.

Transthoracic echocardiography

Transthoracic echocardiography was performed using a GE vivid7 ultrasound machine with a 12-MHz transducer (GE Healthcare, NJ, USA). Basal (Day-0), Day-14 and terminal (Day-28) echocardiography was performed to assess the ventricular dimensions, functions and pulmonary artery flow. Animals were anaesthetised with 2% isoflurane-oxygen mixture. Echo measurements were recorded at the parasternal short-axis view at the papillary muscle level to study the ventricular geometry and function. At this level, M-mode recordings were measured to investigate the left ventricular cardiac function and to determine cardiac dimensions. Ejection fraction was calculated for both RV and left ventricle (LV) and is presented as the ratio of right *versus* left, [RV/LV ejection fraction (EF)]. EF was calculated using the following formula: (end diastolic volume – end systolic volume/end diastolic volume) × 100. In the parasternal short axis view, the transducer was slightly angled to record the video of both RV and LV and this video was used to analyse the right and left ventricular end diastolic area. End diastolic area (EDA) is also presented as ratio between RV and LV. Pulsed Doppler recordings were performed at parasternal short-axis view at the base of heart to measure the right ventricle outflow tract (RVOT) blood flow [right ventricular outflow tract, maximum velocity ($RVOT_{Vmax}$), $m{\cdot}s^{-1}$]. $RVOT_{Vmax}$, is the maximum velocity of blood flow through RVOT. RVOT is the region of the RV, which carries blood from the RV to the pulmonary artery in the anterior-superior direction. Pulmonary artery acceleration and ejection time (A_T and E_T) were calculated from Doppler images. A_T is the time duration between the onsets of blood flow and peak flow velocity in the RVOT, while E_T is the total time required for one cycle of blood flow in the RVOT. Further, Doppler images were assessed for the appearance of midsystolic notches, which is prominent in PH. ECG recordings were performed simultaneously during all ECHO assessments. All the ECHO recordings were performed in triplicates. Three consecutive cycles from each recording (total 9 cycles) was randomly chosen for the assessment of each parameter. Following echo assessments, haemodynamics were measured.

Haemodynamic measurements

Right ventricular systolic pressure (RVSP) was measured using a fluid-filled silastic catheter. In brief, rats were anaesthetized by a single s.c injection of a ketamine/xylazine cocktail (30 $mg{\cdot}kg^{-1}$ and 6 $mg{\cdot}kg^{-1}$, respectively). The silastic catheter connected to a pressure transducer that was interfaced to a PowerLab (AD Instruments, Colorado Springs, CO, USA) signal transduction unit was inserted inside the right descending jugular vein and advanced to the RV. The waveform was used to confirm the positioning of the catheter in the RV; subsequently, wave signals of RVSP were recorded. RVSP was calculated from the recordings using the Lab Chart programme supplied along with PowerLab system. Following the RVSP measurement, animals were killed, and the organs were harvested for RNA, protein, histology and hypertrophy assessments.

Right ventricular hypertrophy assessment (Fulton's index)

Immediately after RVSP measurements, a thoracotomy was performed; after exsanguination, heart and lungs were removed. To calculate right ventricular hypertrophy (RVH), the wet weight of RV and LV + intra ventricular septum (S) was determined. RVH was expressed as the ratio of RV/(LV + S).

Collagen estimation – hydroxyproline assay

A hydroxy proline assay was performed to assess collagen in the whole lungs. In brief, all five lobes of each animal were dried at 65°C for 3 h, weighed and subjected to the collagen estimation as explained in the kit (Biovision, Milpitas, CA,

USA). The presence of total collagen in the all five lobes is expressed as a molar concentration.

Real-time RT-PCR analysis

Real time RT-PCR was used to study the mRNA expression of cytokines *viz.* TNFα, IL-1β, IL-6, inducible NOS, IL-10, IL-13, collagen type 1 (COL1), collagen type 3 (COL3), connective tissue growth factor (CTGF), MMP12, tissue inhibitor of metalloproteinases-1 (TIMP-1), stromal derived factor-1α (SDF-1α), G-CSF, monocyte chemotactic protein-1 (CCL2) and GFP. Total RNA was isolated from punched tissues using TRIzol reagent (Invitrogen Corporation, Carlsbad, CA, USA) according to the manufacturer's specifications. In addition, RNA samples were treated with DNase I (Ambion Inc, Austin, TX, USA) to remove any genomic DNA. First strand cDNA was synthesized from 2 μg RNA with iScript cDNA synthesis kit (Bio-Rad Laboratories, Hercules, CA, USA). Real-time RT-PCR was performed either in 96-well or in 384-well PCR plates using iTaq SYBR Green Super mix with ROX (Bio-Rad) or Taqman Gene Expression System (Life Technologies) in triplicate using the ABI Prism 7900 sequence detection system (Applied Biosystems Corporation, Foster City, CA, USA). The PCR cycling conditions were as follows: 50°C for 2 min, 95°C for 3 min, followed for 45 cycles (15 s at 95°C, and 1 min at 60°C). To confirm the specific PCR product, a dissociation step (15 s at 95°C, 15 s at 60°C, and 15 s at 95°C) was added to check the melting temperature. Gene expression was measured by the ΔΔCT method, and data are presented as relative fold change that of control animals. Primers used in this study can be found in the Supporting Information Table S1.

Immuno histochemical analysis (IHC)

Subsequent to RVH assessment, RV and a lung lobe were processed immediately for the histological analysis. A single lobe of left lung was perfused with PBS followed by 10% neutral buffered formalin and stored in formalin overnight. Similarly, RV was fixed and stored in formalin. The following day, the fixed tissues were rinsed in 70% alcohol and processed for paraffin embedding. Paraffin embedded tissue samples were sectioned (4 μm), de-paraffined and stained with picro sirius (PS) or haematoxylin–eosin (H&E). For the fibrosis staining, images were photographed at 10× magnification. A minimum of 10 non-overlapping images from randomly chosen fields was obtained. IMAGE J software (National Institutes of Health, Bethesda, MD, USA) was used for analysis. In brief, the images obtained were converted to an 8 bit black and white image, and a threshold was identified or adjusted for the fibrosis, using the control lung or RV; this threshold level is maintained when assessing the lung or RV fibrosis across all the experimental groups. Results from each animal were averaged for subsequent statistical analysis. To investigate the pulmonary vessel wall thickness, sectioned lung specimens were stained for α-smooth muscle actin (1:1000, clone 1 A4, Sigma Aldrich), incubated in avidin and stained with Sigma*Fast* 3,3′-diaminobenzidine for a minute; αSMA-positive smooth muscle cells stains brown in colour. Vessels with an external diameter of < 50 μm were considered for the assessment. A minimum of 8–10 vessels were photographed and analysed, and results from each animal were averaged. The % medial wall thickness was calculated using the formula: % medial wall thickness = [(medial thickness × 2)/external diameter] × 100 ($n = 5$ rats per group). Media thickness was defined as the distance between the lamina elastica interna and lamina elastica externa. Images were analysed using the IMAGEJ programme from the National Institutes of Health. To investigate the lung tissue remodelling, sectioned lung specimens were stained with H&E. A minimum of 10–12 non- overlapping images were randomly chosen and photographed at 10×. The blinded Ashcroft scoring (Ashcroft *et al.*, 1988) system was adopted to grade the tissue remodelling across all the experimental groups. Results of each animal were averaged for subsequent statistical analysis.

Immuno fluorescence analysis (IF)

For identification of eGFP-ASCs, paraffin embedded (4 μm) ASC treated MCT lung sections were de-paraffined. De-paraffined lung sections were subsequently incubated in the hybridization buffer containing anti-chicken GFP antibody (1:250) at 4°C overnight. After the overnight incubation, the slide was incubated with the corresponding secondary antibody. Subsequently, a drop of DAPI, the nuclear staining (Vectashield) mounting medium was added, and a cover slip was laid over the lung section. The presence of eGFP-ASCs in the pulmonary vasculature was observed under 400× magnification, in 10 randomly chosen fields for each animal. Images taken using the green channel (GFP), and blue (DAPI) were merged using the IMAGE J software to produce the composite or merged image. Scale bar is 50 μm.

For identification of pericytes, paraffin embedded (4 μm) lung sections were de-paraffined and incubated in sodium citrate (pH – 6.0) at 80°C for 20 min for antigen retrieval. Subsequently, lung sections were incubated in 0.4% triton X in PBS for 30 min and blocked in the 0.1% triton X in PBS containing 2% bovine albumin and 5% normal goat serum for an hour. Following this, the sections were incubated in the 0.1% triton X in PBS containing 2% bovine albumin and 1% normal goat serum, αSMA (1:1000), NG2 (1:350) for overnight at 4°C. The following day, the sections were incubated in the secondary antibody conjugated with goat anti-mouse Texas Red 594 and goat anti-rabbit Alexa Fluor 488 for an hour, washed with 0.1% Triton-X and mounted in the Vectashield DAPI mounting medium. Images were taken using Olympus DSU Spinning Disc Confocal Fluorescent Microscope running on SLIDEBOOK version 4.2 (Intelligent Imaging Innovations Inc, Denver, CO, USA). Z stack images were generated on water-based 60× objective lens. All the images were processed and analysed using the SLIDEBOOK version 4.2. For the image analysis, the NG2 stained cells covering the (DAPI stained) nucleus were counted using SLIDEBOOK version 4.2. For the statistical analysis, 10 vessels per lung section were imaged, and the cell numbers were averaged for each animal and averaged per group. Each group had five animals. Scale is 25 μm.

Western blot analysis

After the animals had been killed, each lobe of the right lung was frozen for the protein work. The frozen right lung was homogenized in radioimmunoprecipitation assay (RIPA) buffer supplemented with protease inhibitor cocktail (Sigma Aldrich). Protein concentration was estimated by the Bradford method. Equal amounts of protein (30 μg for TLR-4 and 50 μg for TGFβ) were separated on 4–20% Mini-PROTEAN TGX gel and transferred electrophoretically onto a nitrocellulose membrane. The membranes were blocked with 5% non-

fat milk solution in Tris-buffered saline (TBS) with 0.1% Tween 20 (TBS-T) for 1 h. Subsequently, the membranes were probed with the primary antibodies, anti-mouse TLR antibody (3 $\mu g \cdot mL^{-1}$), anti rabbit TGFβ antibody (1:1000 dilution), anti-mouse β actin antibody (1:10 000) overnight at 4°C. On the following day, the membranes were incubated with horseradish peroxidase conjugated goat anti-mouse (1:10 000) and goat anti-rabbit (1:10 000) and detected with an enhanced chemiluminescence substrate (GE Healthcare Bio-Sciences, Pittsburgh, PA, USA) and exposed to a photographic film. Developed film was scanned and the mean pixel density of the images was analysed using the IMAGE J software.

Statistics

Data and statistical analysis comply with the recommendations on experimental design and analysis in pharmacology (Curtis *et al.*, 2015). GRAPH PAD PRISM, version 6.0 (La Jolla, CA, USA) was used for statistical analysis. Two-way ANOVA test was performed to analyse the statistical significance between treatment and time, wherever MCT treatment was monitored for 4 weeks. One-way ANOVA data analysis followed by Newman–Keuls test for multiple comparisons was performed for end point parameters of the experiments. The *post hoc* tests were performed only when the *F*-value was significant $P < 0.05$, and there was no significant variance in homogeneity. Values are represented as means ± SEM, *P* values of ≤ 0.05 were considered statistically significant. Since the preliminary experiments in the MCT or Bleo studies were performed to identify the best time to administer our therapeutic agents, fewer animals (MCT, $n = 6$ and Bleo, $n = 5$, each group) were utilized. However, for all the subsequent experiments each group comprised of $n = 8$ animals based on our preliminary studies and power analysis. Nonetheless, '*n*' values in the experimental endpoints differed from the initial design because of invalid tracings or animal death during haemodynamic assessment or ASC/CM administration. As RNA integrity is the critical step for RT-PCR analysis, we decided to use only those RNA samples exhibiting an absorbance ratio (260/280) of more than 1.8. As a consequence, the '*n*' was reduced to 4 for some of our experimental groups. For histology, RT-PCR and western blot analysis, randomly chosen lung/hearts ($n = 5$, each group) were utilized in both MCT and Bleo experiments, unless specified.

Reagents, antibodies and chemicals

Monocrotaline (MCT), α-smooth muscle actin (clone 1 A4) and β-actin (clone AC-15) antibodies were purchased from Sigma Aldrich (St. Louis, USA). Anti-GFP chicken antibody was procured from Aves Lab (Tigard, OR, USA). NG2, TLR-4 and TGFβ (KLH coupled synthetic peptide) antibodies and bleomycin were purchased from EMD Millipore (Billerica, MA, USA), Abcam (Cambridge, MA, USA), and Cell Signalling Technology (Danver, MA, USA), respectively. Goat anti-mouse Texas Red 594 and goat anti-rabbit Alexo Fluor 488 were purchased from Life Technologies, NY, USA. Anti-rat CD34, CD44, CD45 and CD90 were obtained from AbD Serotec (Raleigh, NC, USA), and the corresponding isotype matched antibodies were procured from Sigma Aldrich. FBS was obtained from Atlanta Biologicals (Flowery Branch, GA, USA). DMEM and antibiotic solution were purchased from Cellgro (Manassas, VA, USA). Cytokine array kit was purchased from R&D systems (Minneapolis, MN, USA). Photographic film was purchased from Denville Scientific (South Plainfield, NJ, USA). A 4–20% Mini-PROTEAN TGX gel was procured from Bio-Rad Laboratories (Hercules, CA, USA). Dermal fibroblasts were purchased from Cell Applications (San Diego, CA, USA). All tissue culture requirements were purchased from Corning (Tewksbury, MA, USA).

Results

Characterization of rat adipose stem cells (ASCs)

We performed flow cytometry to characterize the mesenchymal origin of ASCs. ASCs stained positive for the MSC markers, CD44 (56%) and CD90 (92%), negative for the haematopoietic stem cell marker CD34, while CD45 (0.8%), the leukocyte marker was observed in traces (Figures 1A–D). Further, the differentiation assay was performed where ASCs were differentiated to adipocytes, osteocytes and chondrocytes by chemical induction (Figures 1E–H).

ASCs or CM treatment arrest the progression of PH by improving ventricular dynamics and attenuating cardiac remodelling

In the preliminary study, RV dynamics and cardiac function was measured every 2 weeks. MCT-challenged rats demonstrated a significant elevation of RVSP after 2 weeks ($P \leq 0.05$), which continued to rise ($P \leq 0.05$) at 4 weeks (Figure 2A). Further, the Fulton's index (RV/LV + S) signified a gradual increase in the RV hypertrophy ($P \leq 0.05$) in the MCT animals (Figure 2B). ECHO assessments demonstrated a gradual enlargement of the RV and a concomitant shrinking of the LV, resulting in structural modifications ($P \leq 0.05$) in the MCT animals (Figure 2C-D and Supporting Information Movies S1–5 and 7). Eventually, this ventricular remodelling resulted in a significant reduction in the RV/LV ejection fraction ($P \leq 0.05$) in the MCT animals (Figure 2E). Doppler ECHO was performed to assess the pulmonary blood flow. MCT-insult steadily decreased the A_T/E_T ($P \leq 0.05$), with an appearance of a mid-systolic notch in the Doppler wave, which eventually blunted the pulmonary blood flow (Figures 2F–H). Since significant pathological damages were observed on Day-14, we decided to administer ASCs or CM 2 weeks post MCT-insult.

Two weeks after jugular vein administration of eGFP-ASCs or CM, RVSP (Figure 3A) was significantly reduced ($P \leq 0.05$). In addition, the increased right ventricular end diastolic pressure (RV EDP) was also significantly reduced in ASCs or CM groups (Figures 3B). Similar to the haemodynamic data, ECHO assessments demonstrated that ASCs or CM arrested ventricular remodelling, improved cardiac function and enhanced pulmonary blood flow in the MCT animals (Table 1, Supporting Information Figure S1 and Supporting Information Movies S6 and 8). Consistent with other pathological changes, the interstitial collagen deposition (Picro Sirius staining) observed in the RV of MCT animals was also considerably decreased by ASCs or CM treatment (Figures 3C and D). Furthermore, the altered RV hypertrophy associated with the PH animals was also significantly attenuated in the two

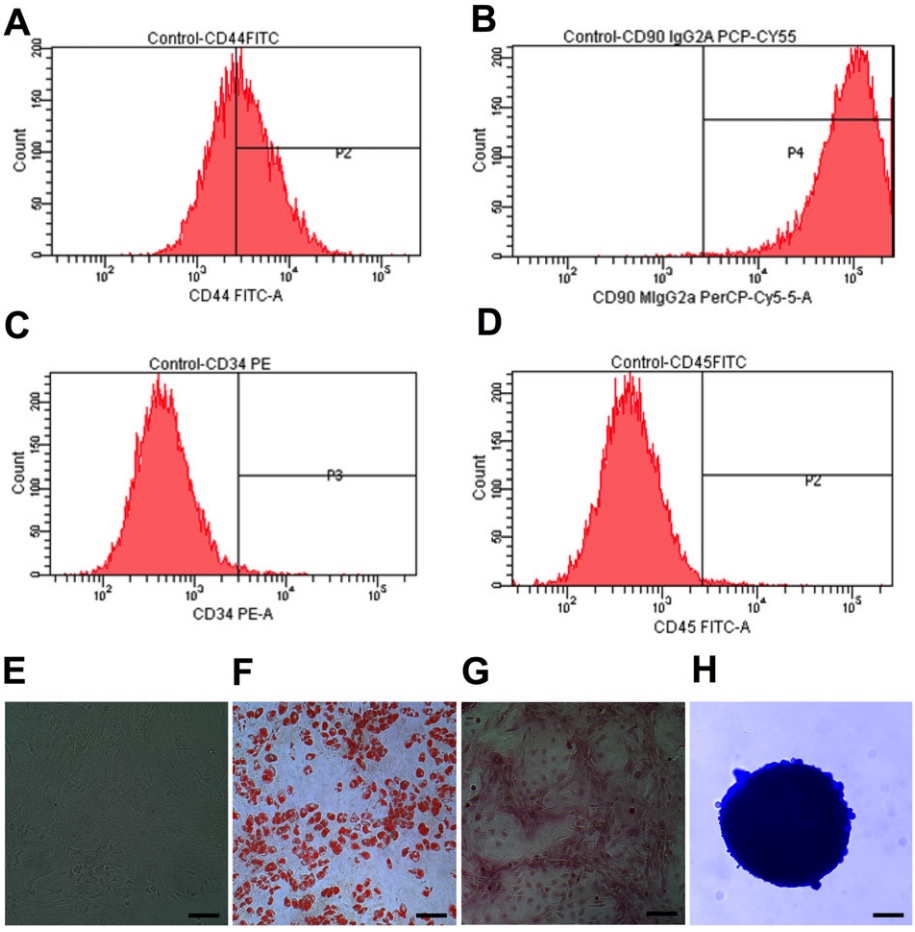

Figure 1

Characterization of ASCs; 0.5 × 10^6 of cultured ASCs at passage 2 were labelled with antibodies of specific cell surface phenotype markers for 30 min at 4°C and subjected immediately to flow analysis. Data represent the flow analysis of (A) CD44, (B) CD90, (C) CD34 and (D) CD45. (E) ASCs resembled fibroblast in morphology. Cells were imaged, under bright field microscopy. (F) Adipocyte staining by Oil Red 'O'. (G) Osteocyte staining by Alizarin Red. (H) Chondrocyte staining by Alcian Blue. Scale bar = 100 μm.

treatment groups (Figure 3E). We repeated this study with DF or DF-CM to ensure the specific therapeutic benefits of ASCs or CM. As expected, DF or DF-CM did not elicit any improvement in RVSP or RVH (Supporting Information Figure S2 A and B).

ASCs or CM treatment improves the pulmonary vascular remodelling associated with PH

To investigate the muscularization of pulmonary vessels, lung sections were stained with α-smooth muscle actin (αSMA). IHC analysis demonstrated the muscularization (2.7 fold) of the pulmonary vessels (< 50 μm) in the PH animals, while ASCs or CM treatment arrested this event (Figures 4A and C). To assess the pulmonary pericyte coverage, we stained the lung sections with NG2 (pericyte) and αSMA. Pericytes are polymorphic in nature, and they were counted based on the nucleus encompassed by green stain. Distribution of pericytes (white arrows) around the endothelial lumen (L) was abundant in the MCT-injected animals (Figures 4 B.g, and B.k). Treatment with either ASCs or CM significantly reduced the distribution of pericytes (Figures 4 B.o and B.s). Further, the abundant distribution of αSMA stained cells in the MCT-injected animals was also diminished in the presence of ASCs or CM (Figures 4 B.d, B.h, B.l, B.p and B.t). Collectively, our results demonstrated that ASCs or CM treatment equally improve pulmonary vascular remodelling in PH (Figure 4D).

ASCs or CM modulate the cytokines involved in the pathogenesis of PH

Real-time RT-PCR and Western blot experiments were performed to study the effect of ASCs or CM on pulmonary cytokines. Expression of markers of inflammation (TNFα; 4.3, IL-1β; 3.7 and IL-6; 12.3 folds), immune defence system (TLR-4; 2.6 and iNOS; 3.4 fold) and tissue remodelling (TGFβ, both precursor and matured protein; 4.7 fold) were significantly up regulated in the MCT-injected animals (Figures 5A-H). Furthermore, MCT animals exhibited a decrease in the expression of the anti-inflammatory cytokine IL-10 (Figure 5I). Our findings demonstrated that treatment of PH animals with ASCs decreased the expression of markers associated with inflammation, immune

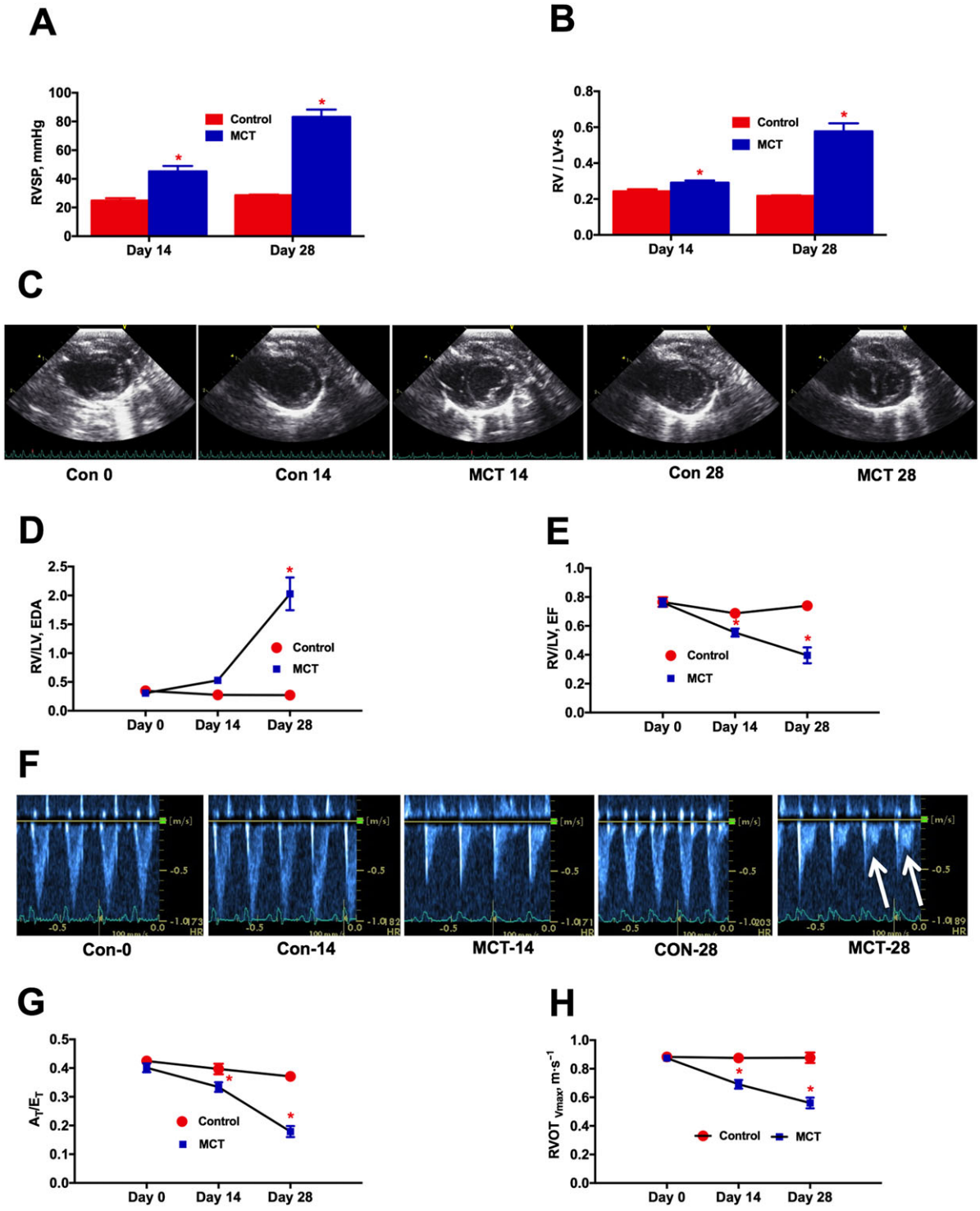

Figure 2

Time course analysis of PH-induced dysregulation of ventricular and pulmonary vascular remodelling. At 0, 14 and 28 days following the MCT-insult, animals were monitored for haemodynamic and cardiac parameters. (A), and (B) represent the kinetic profile of RVSP and RVH, respectively, in controls and MCT-challenged rats. RVH is the ratio of RV to LV + S weights, [RV/(LV + S)]. (C) Parasternal short axis view of the ventricles for control and MCT animals on Day-0, Day-14 and Day-28, demonstrating a shift in the IV septum. (D) Kinetic profile of RV/LV EDA in controls and MCT-challenged rats. RV/LV EDA is the ratio of RV *versus* LV EDA. (E) Kinetic profile of RV/LV EF in controls and MCT-challenged rats. RV/LV EF is the ratio of RV EF *versus* LV EF and EF is the ejection fraction. (F) Image of pulsed Doppler recordings. Mid-systolic notch is observed in the MCT animals, as indicated by the white arrows. (G) and (H) represent the kinetic profile of A_T/E_T and $RVOT_{Vmax}$ in the advancement of PH. A_T/E_T is the ratio of acceleration time (A_T) *versus* ejection time (E_T). $RVOT_{Vmax}$ is the velocity of pulmonary blood flow in the RVOT. Data presented in (A), (B), (D), (E), (G) and (H) are mean ± SEM (n = 6). * P value of ≤ 0.05 when comparing MCT treatment against controls.

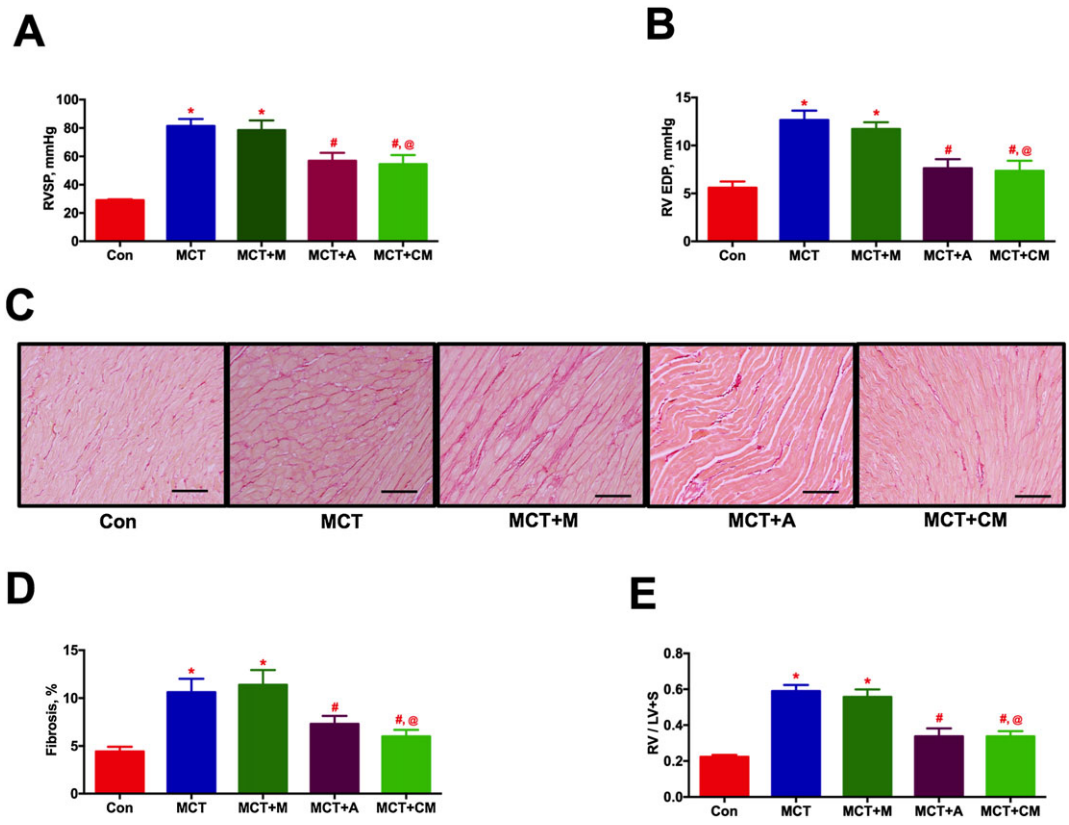

Figure 3

ASCs treatment improves the ventricular dynamics and cardiac function in PH in a paracrine fashion. ASCs or CM were injected through the jugular cannula, 2 weeks following MCT-insult. Following 4 weeks of MCT-injection, ventricular haemodynamics, cardiac function and RV fibrosis were measured. (A) and (B) represent the improvement in haemodynamic parameters, RVSP and RV EDP, in MCT animals in the presence of ASCs or CM. (C) Representative images of RV fibrosis by PS staining. Scale bar = 200 μm. (D) Attenuation of RV fibrosis in the MCT animals by ASCs or CM treatment. (E) Reduction in MCT-induced RVH by ASCs or CM therapy. Data presented in (A), (B), and (E) are mean ± SEM (n = 8). Data presented in (D) are mean ± SEM (n = 5). * P value of ≤ 0.05, comparing MCT and MCT + M *versus* control. # P value of ≤ 0.05, comparing MCT + A and MCT + CM *versus* MCT. @ P value of ≤ 0.05, comparing MCT + CM *versus* MCT + M.

Table 1

ASCs or CM attenuates cardiac and pulmonary vascular remodelling associated with PH

	Con (n = 8)	MCT (n = 8)	MCT + M (n = 5)	MCT + A (n = 8)	MCT + CM (n = 8)
RV/LV EDA	0.29 ± 0.02	2.03 ± 0.28[a]	1.91 ± 0.37[a]	0.68 ± 0.17[b]	0.59 ± 0.06[b,c]
RV/LV EF	0.74 ± 0.02	0.37 ± 0.06[a]	0.35 ± 0.03[a]	0.63 ± 0.03[b]	0.56 ± 0.04[b,c]
A_T/E_T	0.37 ± 0.01	0.18 ± 0.02[a]	0.19 ± 0.01[a]	0.33 ± 0.02[b]	0.30 ± 0.01[b,c]
RVOT V_{Max}	0.87 ± 0.03	0.56 ± 0.03[a]	0.55 ± 0.05[a]	0.74 ± 0.03[b]	0.76 ± 0.02[b,c]

ASCs or CM were injected via a jugular cannula, 2 weeks following the MCT insult. Following 4 weeks of MCT treatment, ECHO parameters were assessed. Data demonstrate the improvement in cardiac function, RV/LV EDA and RV/LV EF and pulmonary blood flow, A_T/E_T and $RVOT_{Vmax}$ by ASCs or CM in PH. Data presented are mean ± SEM, Con (n = 8), MCT (n = 8), MCT + M (n = 5), MCT + A (n = 8) and MCT + CM (n = 8).

[a] $P \leq 0.05$, comparing MCT and MCT + M *versus* control.

[b] $P \leq 0.05$, comparing MCT + A and MCT + CM *versus* MCT.

[c] $P \leq 0.05$, comparing MCT + CM *versus* MCT + M.

defence or tissue remodelling and increased the expression of anti-inflammatory cytokine, IL-10. Likewise, CM treated animals also elicited similar protective effects, but in an iNOS-independent fashion. The elevated expression of SDF-1α (3.5 fold) or G-CSF (5.6 fold), which primarily mobilizes the pro-inflammatory; progenitor/stem cells to the injured site were also significantly attenuated in presence of ASCs or CM (Figures 5J and K).

Presence of eGFP-ASCs in the PH lung

After the animals had been killed, lung sections were stained with GFP antibody to detect the presence of eGFP-ASCs. Lung sections were randomly analysed at multiple fields (10 fields per animal). IHC study demonstrated the presence of ~2–3 eGFP-ASCs (2.61 ± 0.43) per field and ~25 (24.7 ± 1.45) eGFP-ASCs per lung section of the MCT animals treated with cells (Supporting Information Figure S3 A-D). Furthermore, we performed real time RT-PCR experiments to confirm the presence of eGFP. The GFP product was observed around the 10th cycle in the eGFP-ASCs administered MCT animals, while no signal was observed in the controls. The housekeeping product GAPDH was observed around the 23rd cycle in all the experimental groups (Supporting Information Figure S3E). These observations signify a slight presence of eGFP-ASCs in the MCT lung.

Kinetics of bleomycin-induced PH

In the preliminary study, following 3, 7, and 14 days of Bleo-instillation, a subset of animals from each group was killed and lung sections were stained with PS or H&E. PS staining demonstrated a moderate but significant appearance of collagen fibres after 3 days and a significant accumulation after 7 and 14 days ($P \leq 0.05$). Consistent with the PS, H&E staining also demonstrated an extensive lung tissue remodelling ($P \leq 0.05$) in the Bleo animals (Figures 6A-D). Based on the histological analysis, a significant structural modification of lung architecture was observed after 3 days, which was intensified with time. Therefore, we decided to administer ASCs or CM either after 3 (early) or 7 (late) days of Bleo-instillation.

ASCs or CM treatment attenuates lung tissue remodelling and secondary PH in Bleo-induced PF (early phase)

In the early phase study, ASCs or CM were administered via the jugular vein after 3 days of Bleo-instillation. Following 2 weeks of Bleo-instillation, haemodynamics were measured, animals were killed and lung sections were stained with PS or H&E. IHC analysis of lung sections demonstrated an extensive PS staining (in the Bleo lungs (Figures 7A and C). This collagen deposition was verified in the subsequent study where whole lung hydroxyproline content was determined (Figure 7D). In addition, a significant tissue remodelling was observed in the Bleo animals (Figures 7B and E). Treatment with either ASCs or CM equally prevented the collagen deposition and lung tissue remodelling associated with the PF animals (Figures 7A–E). The Bleo-treated animals developed secondary PH, RV hypertrophy and cardiac dysfunction, which were all significantly reduced with ASC or CM treatment (Table 2).

ASCs or CM treatment arrests lung tissue remodelling and secondary PH in Bleo-induced PF (late phase)

In the late phase study, cells or CM was administered after 7 days of Bleo-instillation. All the end points were assessed as described in the early phase study. Similar to the early phase study, lung fibrosis, tissue remodelling, collagen accumulation, secondary PH and cardiac dysfunction associated with the Bleo animals were all significantly arrested in the presence of ASCs or CM (Figures 8A–F, and Table 3).

ASCs or CM treatment reduce the fibrotic, tissue remodelling and inflammatory markers in PF (early and late phase)

As with the PH study, real-time RT-PCR measurements were performed on the lung samples after 2 weeks of Bleo administration. Primary targets involved in the fibrogenesis (CTGF; 7 fold), tissue remodelling (IL-13; 5, MMP12; > 18, and TIMP1; 4 fold), and inflammation (CCL2; > 11, and IL-6; 5 fold) were all significantly up-regulated in the Bleo lungs (Figures 9A–F, and Table 4). Many of these parameters increased further with time after administration of Bleo (Table 4). Either ASCs or CM treatment in both the early (Figure 9A-F) and late (Table 4) phase groups attenuated the expression of all these targets. Key markers of collagen synthesis (COL1; 5 and COL3; 3 folds) were also significantly elevated in the PF lungs (Figures 9G and H). ASCs demonstrated a trend in attenuating the expression, while CM treatment significantly attenuated COL1 and COL3 in the early phase group. Either the expression of COL1 or COL3 was not significantly reduced with ASC or CM treatment in the late phase group (Table 4).

Characterization of the ASCs-CM

In order to characterize the contents of CM, we performed a cytokine array assay. A total of 200 μg (285 μL) of CM was used for the cytokine analysis. A total of 285 μL of concentrated plain media (without serum) was used as a control. Cytokine profiling demonstrated the presence of chemokines (CINC-1, CINC-2α, sICAM, LIX, MIP-1α and MIP-3α), TIMP-1 and VEGF (Figures 10A–C) in the CM of ASCs.

Discussion

Although there have been recent reports demonstrating beneficial effects of adipose stem cell therapy in models of PH and PF (Eguchi *et al.*, 2014; Lee *et al.*, 2014; Somanna *et al.*, 2014; Luo *et al.*, 2015), this is the first report to demonstrate that the secretions of ASCs also result in similar therapeutic effects in these diseases. This concept that secretions from stem cells may be responsible for the observed beneficial effects of stem cell therapy is now a prevalent theory (Blaber *et al.*, 2012; Sabin and Kikyo, 2014). Recently Salgado *et al.* (2010) identified several soluble factors within the ASC secretomes, some of which are similar to those observed in our CM. The fact that the CM from ASCs elicits therapeutic improvement of both cardiac and pulmonary pathophysiology in the MCT and Bleo models are supported by several studies that have utilized secretions of ASCs to treat other pathophysiological conditions. In an *in vitro* study, Ribeiro *et al.* (2012) demonstrated that secretions from ASCs could ameliorate neuronal injury in primary cultures. Jeon *et al.* (2013) also demonstrated a neuroprotective effect of extracts from ASCs in experimental stroke models. Cytosolic extracts from ASCs have also been shown to protect mice from epilepsy (Jeon *et al.*, 2011), whereas neither boiled ASCs extract nor extract from fibroblasts produced any such protective effects in this epilepsy model. Likewise, dermal fibroblast or CM from these cells did not produce any beneficial effect in the MCT-

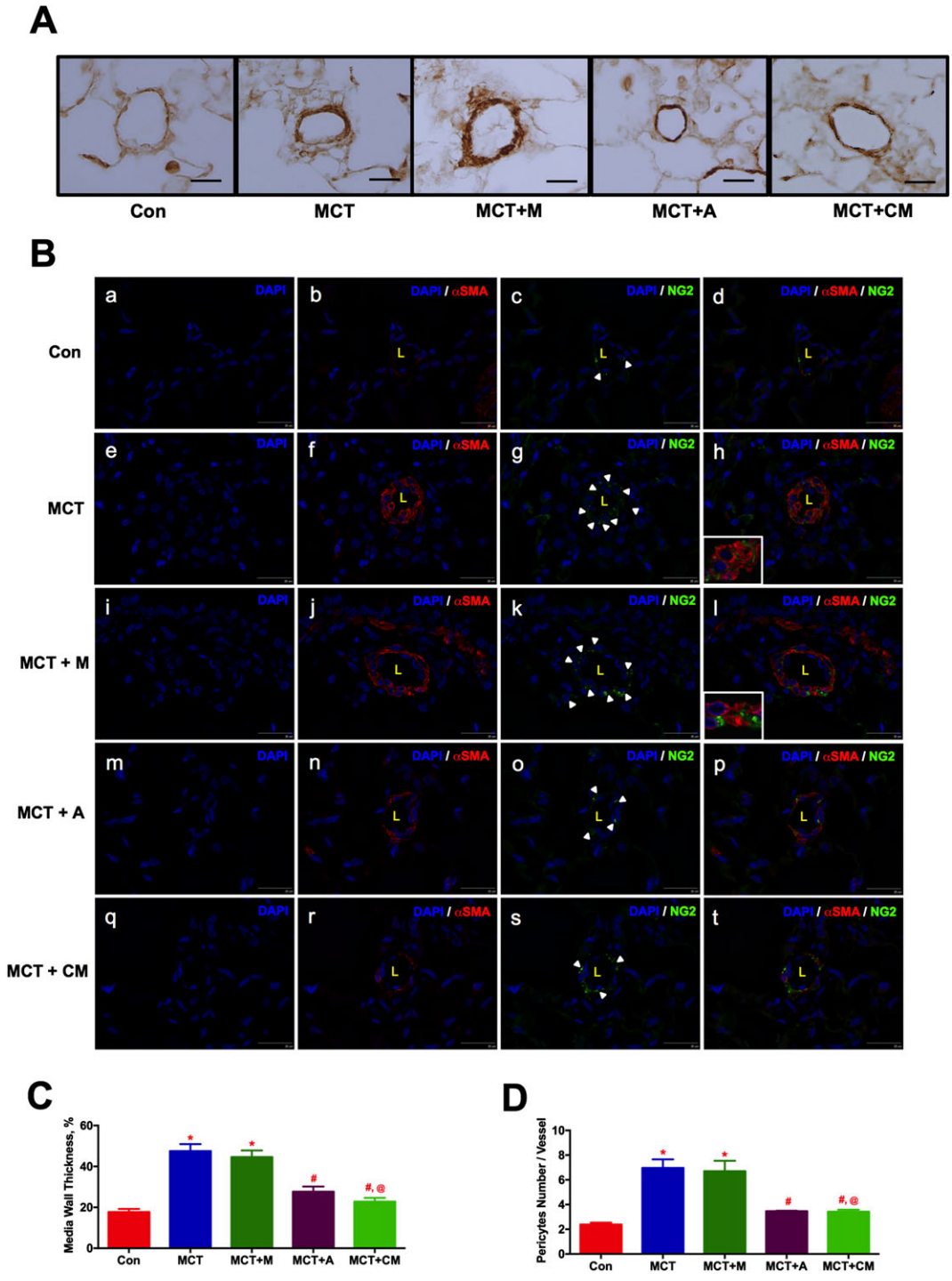

Figure 4

ASCs treatment improves pulmonary vascular remodelling in PH in a paracrine fashion. ASCs or CM were injected via a jugular cannula, 2 weeks following the MCT insult. Following 4 weeks of MCT-insult, pulmonary vessel wall thickness was assessed by IHC and IF staining. (A) Pulmonary vessel wall thickness. (B) Pericyte coverage; NG2 (green, pericyte marker), αSMA (red, smooth muscle marker). Immunofluorescence images were viewed under a spinning disc confocal microscope. (B.a), (B.e), (B.i), (B.m) and (B.q) represent the DAPI staining. (B.b), (B.f), (B.j), (B.n) and (B.r) represent the αSMA with DAPI staining. (B.c), (B.g), (B.k), (B.o) and (B.s) represent the NG2 with DAPI staining. (B.d), (B.h), (B.l), (B.p) and (B.t) represent the merged image of αSMA and NG2 with DAPI. Inserts in (h) and (l) represent the contact point between αSMA and NG2 stained cells. (C) and (D) represent the pulmonary vessel wall thickness and pericyte coverage in all the experimental groups. Data presented in (C) and (D) are mean ± SEM, (10 randomly chosen fields from each animal and $n = 5$ animals). Scale bar is 25 μm. * P value of ≤ 0.05, comparing MCT and MCT + M *versus* control. # P value of ≤ 0.05, comparing MCT + A, and MCT + CM *versus* MCT. @ P value ≤ 0.05, comparing MCT + CM *versus* MCT + M.

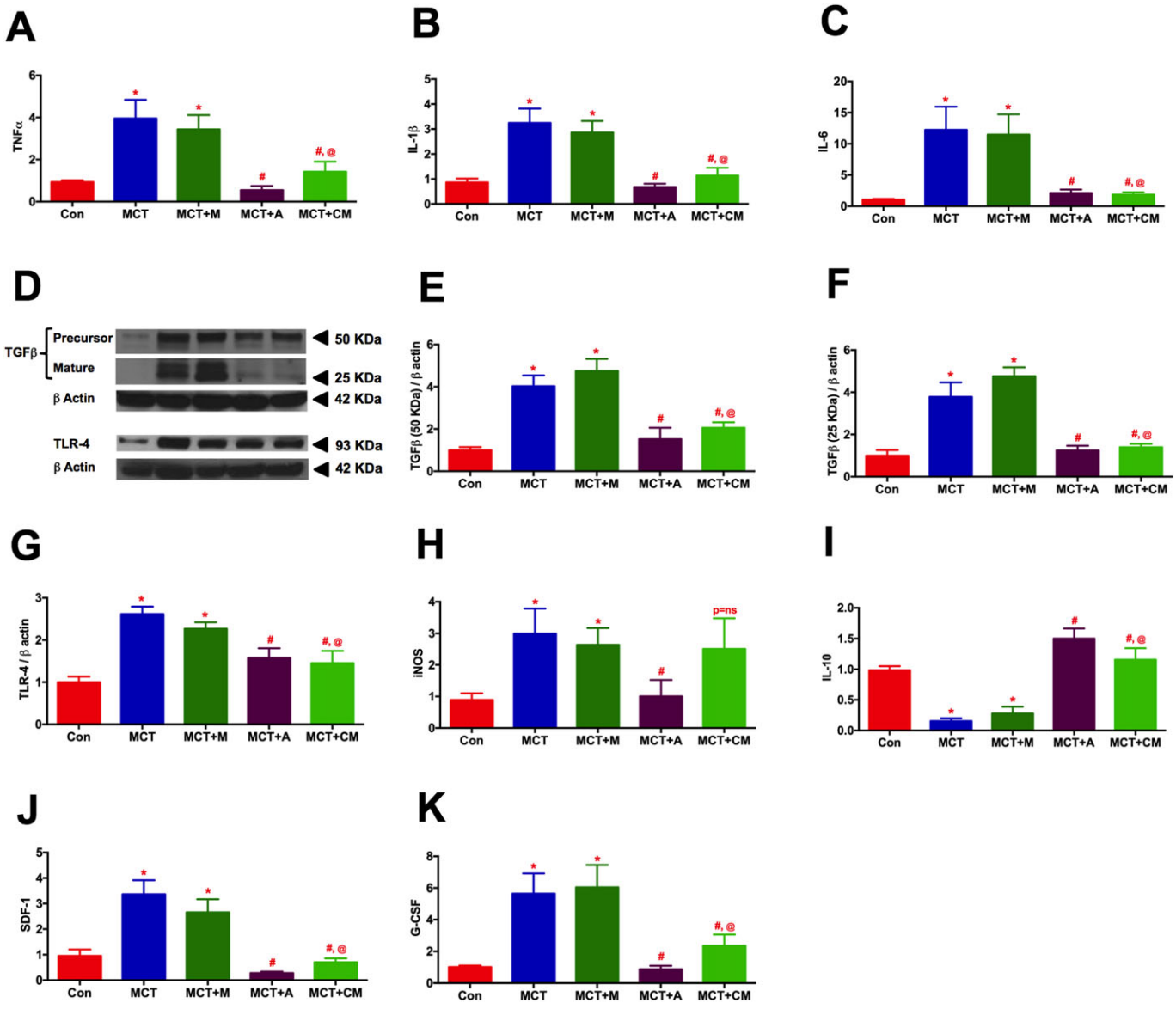

Figure 5

ASCs or CM modulates the expression of pulmonary cytokines in PH. Lung tissue harvested at the termination of the study was analysed for the expression of cytokines by RT-PCR and western blot analysis: (A) TNFα, (B) IL-1β, (C) IL-6, (D) TGFβ and TLR-4, (E) TGFβ (precursor, 50 KDa), (F) TGFβ (mature, 25 KDa), (G) TLR-4, (H) iNOS, (I) IL-10, (J) SDF-1α, and (K) G-CSF. Data presented in (A)–(B) and (D)–(K) are mean ± SEM, $n = 5$ animals per group. The number of animals included per group in (C) are control ($n = 5$), MCT ($n = 5$), MCT + M ($n = 4$), MCT + A ($n = 5$) and MCT + CM ($n = 5$), mean ± SEM. * P value of ≤ 0.05, comparing MCT and MCT + M *versus* control. # P value of ≤ 0.05, comparing MCT + A, and MCT + CM *versus* MCT. @ P value of ≤ 0.05, when MCT + CM is compared against MCT + M.

injected animals, further supporting the view that factors secreted by ASCs is most likely to mediate the observed therapeutic effects. Therefore, the most significant finding of this investigation is that CM from ASCs can arrest the progression of PH or PF by attenuating inflammatory stress, and cardiopulmonary remodelling.

We and others (Brunner *et al.*, 2002; Shenoy *et al.*, 2010; Shenoy *et al.*, 2014) have demonstrated a right heart dysfunction following the induction of PH or PF by MCT or Bleo, respectively. Right heart dysfunction is most likely a result of the increased pulmonary pressure, resulting in elevated cardiac workload (Jone *et al.*, 2014). However, it has been reported (Akhavein *et al.*, 2007) that MCT can also have a direct cardio toxic effect. In our study, treatment with either ASCs or CM provided equivalent beneficial effects on numerous indicators of cardiac function as well as lowering of pulmonary pressures. Therefore, it is possible that the cardio protective effects mediated by our interventions can be a result of either a direct action on the cardiac tissue or a secondary effect caused by lowering of pulmonary pressure, thereby, preserving normal cardiac function, or both. Similar effects were observed in the Bleo model of PF and secondary PH, which confirms the therapeutic efficacy of ASCs or CM against cardiopulmonary diseases.

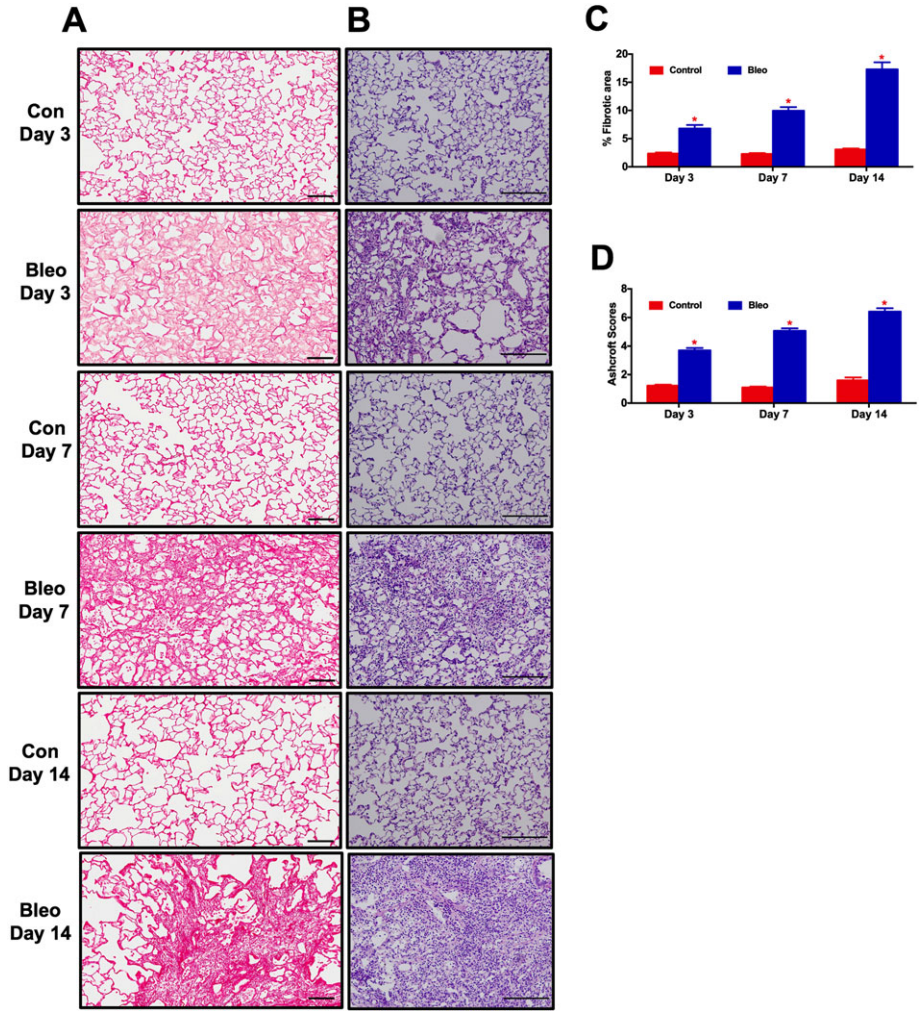

Figure 6

Time course analysis of lung fibrosis and tissue remodelling in the Bleo model. At 3, 7 and 14 days following the Bleo-insult, animals were killed, and the harvested lungs were sectioned and stained with PS or H&E. (A), (C), and (B), (D) represent the kinetic profile of PS and H&E staining, for controls and Bleo-challenged rats. Data presented in (C) and (D) are mean ± SEM (n = 5). *P value of ≤ 0.05 when comparing Bleo treatment against controls.

Pulmonary vascular resistance (PVR) is believed to be associated with hyper-proliferation of endothelial and vascular smooth muscle cells (Sakao *et al.*, 2006), while a recent study suggests a possible role of pericytes in the pathogenesis of PH (Ricard *et al.*, 2014). Endothelial derived IL-6 or FGF-2 are the key factors that transform quiescent pericytes to acquire contractile, hyper-proliferative nature (Ricard *et al.*, 2014), which increases the PVR. Eventually, PVR obstructs the forward pulmonary blood flow and enhances reverse flow from the pulmonary artery to the RV (Dabestani *et al.*, 1987). Interestingly, ASCs or CM treatment of MCT animals reduced IL-6 expression, decreased pericyte coverage and improved the pulmonary blood flow.

Infiltration of immune cells to the injured endothelium increases the release of pro-inflammatory cytokines and the suppression of reported anti-inflammatory cytokine (IL-10) in the PH lung (Bauer *et al.*, 2012; Price *et al.*, 2012). Numerous studies emphasize the critical role of TNFα, TLR-4 and TGFβ in driving pulmonary vascular remodelling, which advances the pathogenesis of PH (Zaiman *et al.*, 2008; Bauer *et al.*, 2012; Hameed *et al.*, 2012). It has been reported that inflammatory macrophages secrete IL-10, when they have a direct contact with stem cells (Nemeth *et al.*, 2009). Further, inhibition of TGFβ results in the generation of IL-10 producing T-helper cells (Dardalhon *et al.*, 2008). Therefore, our findings suggest that ASCs administered to PH animals may similarly result in an increase of IL-10 and suppression of inflammatory signals. Inhibition of iNOS arrests the inflammatory responses in many lung diseases (Hesslinger *et al.*, 2009). This may be one way ASCs mediate some of the beneficial effects against PH. However, since this effect was not observed in the CM treatment, it indicates that the reduction of iNOS may not be the major process that produces the beneficial effects. Similar to PH, infiltration of immune cells to the injured epithelium in PF releases inflammatory signals, which drive the proliferation and differentiation of fibroblasts to myofibroblasts with the concomitant collagen deposition and tissue remodelling (Habiel and Hogaboam, 2014).

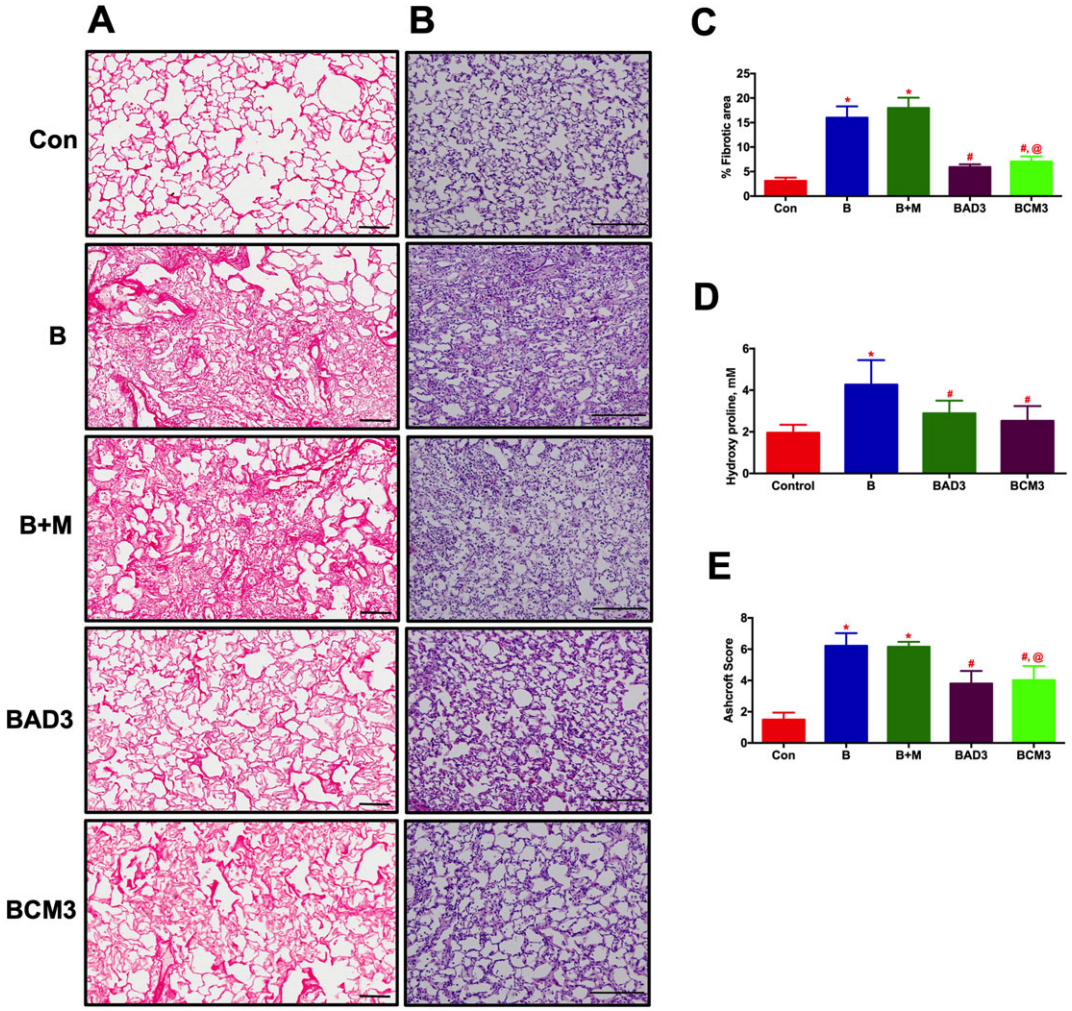

Figure 7

ASCs or CM treatment attenuates lung fibrosis and tissue remodelling in the Bleo animals (Early phase). ASCs or CM were injected through the jugular vein after 3 days of Bleo-instillation. Following 2 weeks of Bleo-instillation, animals were sacrificed, and the lungs were stained with PS and H&E staining to assess lung fibrosis and tissue remodelling. (A) and (C) represent the improvement of pulmonary fibrosis in the Bleo animals in presence of ASCs or CM. Scale bar = 100 μm. (B) and (E) represent the improvement of lung tissue remodelling in the Bleo animals in presence of ASCs or CM. Scale bar = 200 μm. (D) Demonstrates the attenuation of collagen deposition (hydroxyl proline) in the presence of ASCs or CM in the Bleo animals. Data presented in (C)-(E) are mean ± SEM ($n = 5$). * P value of ≤ 0.05, comparing B and B + M animals against the controls. # P value of ≤ 0.05, comparing BAD3 and BCM3 *versus* B. @ P value of ≤ 0.05, comparing BCM3 *versus* B + M.

Table 2

ASCs or CM treatment attenuates the cardiac dysfunction in PF (Early phase)

	Con ($n = 8$)	B ($n = 8$)	B + M ($n = 6$)	BAD3 ($n = 7$)	BCM3 ($n = 8$)
RVSP	28.64 ± 1.04	45.55 ± 2.49[a]	46.98 ± 2.82[a]	33.29 ± 1.59[b]	34.84 ± 3.94[b,c]
RV/LV + S	0.27 ± 0.01	0.40 ± 0.02[a]	0.39 ± 0.02[a]	0.33 ± 0.02[b]	0.32 ± 0.01[b,c]
RV/LV EDA	0.31 ± 0.02	0.64 ± 0.05[a]	0.68 ± 0.05[a]	0.38 ± 0.02[b]	0.36 ± 0.02[b,c]
RV/LV EF	0.71 ± 0.01	0.53 ± 0.04[a]	0.54 ± 0.03[a]	0.65 ± 0.03[b]	0.64 ± 0.02[b,c]

ASCs or CM were injected through the jugular vein after 3 days of Bleo instillation. Following 2 weeks of Bleo instillation, ECHO and haemodynamic parameters were assessed. Data demonstrate the improvement of cardiac function and haemodynamics in the Bleo animals in presence of ASCs or CM. Data presented are mean ± SEM, Con ($n = 8$), B ($n = 8$), B + M ($n = 6$), BAD3 ($n = 7$), and BCM3 ($n = 8$).

[a] $P \leq 0.05$, comparing B and B + M animals against the controls.

[b] $P \leq 0.05$, comparing BAD3 and BCM3 *versus* B.

[c] $P \leq 0.05$, comparing BCM3 *versus* B + M.

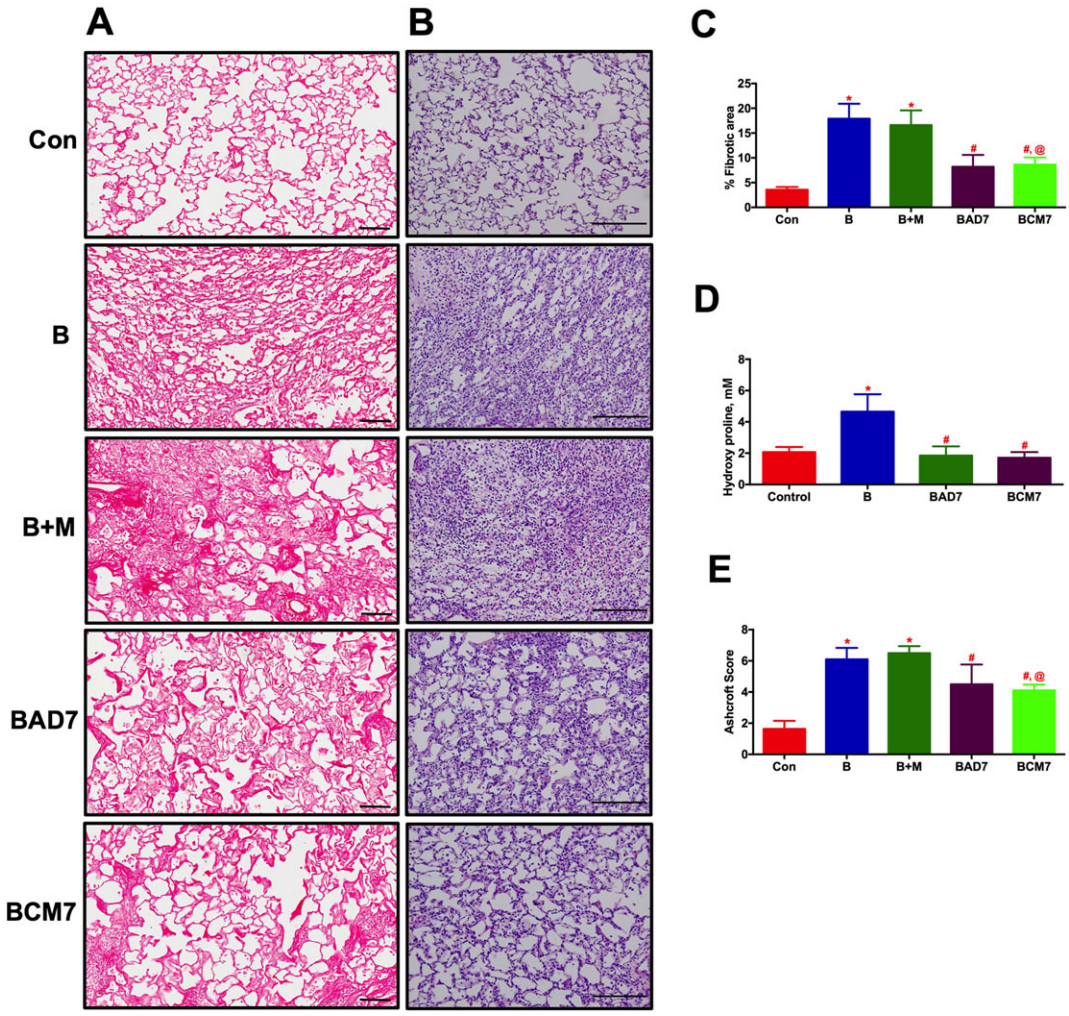

Figure 8

ASCs or CM treatment arrests the progression of established lung fibrosis and tissue remodelling in Bleo animals (Late phase). ASCs or CM were injected through the jugular vein after 7 days of Bleo-instillation. Following 2 weeks of Bleo-instillation, animals were killed, and the lungs were stained with PS and H&E. (A) and (C) represent the anti-fibrotic effects of ASCs or CM. Scale bar = 100 μm. (B) and (E) improvement of lung tissue remodelling in the Bleo animals in presence of ASCs or CM. Scale bar = 200 μm. (D) Attenuation of collagen deposition as measured by lung hydroxyl proline content by ASCs or CM treatment. Data presented in (C)–(E) are mean ± SEM (n = 5). * P value of ≤ 0.05, comparing B and B + M animals against the controls. # P value of ≤ 0.05, comparing BAD7 and BCM7 *versus* B. @ P value of ≤ 0.05, comparing BCM7 *versus* B + M.

Table 3

ASCs or CM treatment arrests the cardiac dysfunction in PF (Late phase)

	Con (n = 8)	B (n = 8)	B + M (n = 6)	BAD7 (n = 7)	BCM7 (n = 7)
RVSP	29.03 ± 1.25	45.71 ± 3.92[a]	48.03 ± 2.76[a]	36.22 ± 2.80[b]	32.11 ± 2.74[b,c]
RV/LV + S	0.25 ± 0.01	0.41 ± 0.02[a]	0.39 ± 0.01[a]	0.32 ± 0.01[b]	0.32 ± 0.01[b,c]
RV/LV EDA	0.31 ± 0.01	0.71 ± 0.04[a]	0.65 ± 0.05[a]	0.37 ± 0.01[b]	0.41 ± 0.02[b,c]
RV/LV EF	0.73 ± 0.01	0.56 ± 0.03[a]	0.53 ± 0.03[a]	0.69 ± 0.04[b]	0.67 ± 0.04[b,c]

ASCs or CM were injected through the jugular vein after 7 days of Bleo instillation. Following 2 weeks of Bleo instillation, ECHO and haemodynamic parameters were assessed. Data demonstrate the improvement in cardiac function and haemodynamics in the Bleo animals in presence of ASCs or CM. Data presented are mean ± SEM, Con (n = 8), B (n = 8), B + M (n = 6), BAD7 (n = 7), and BCM7 (n = 7).

[a] $P \leq 0.05$, comparing B and B + M animals against the controls.

[b] $P \leq 0.05$, comparing BAD7 and BCM7 *versus* B.

[c] $P \leq 0.05$, comparing BCM7 *versus* B + M.

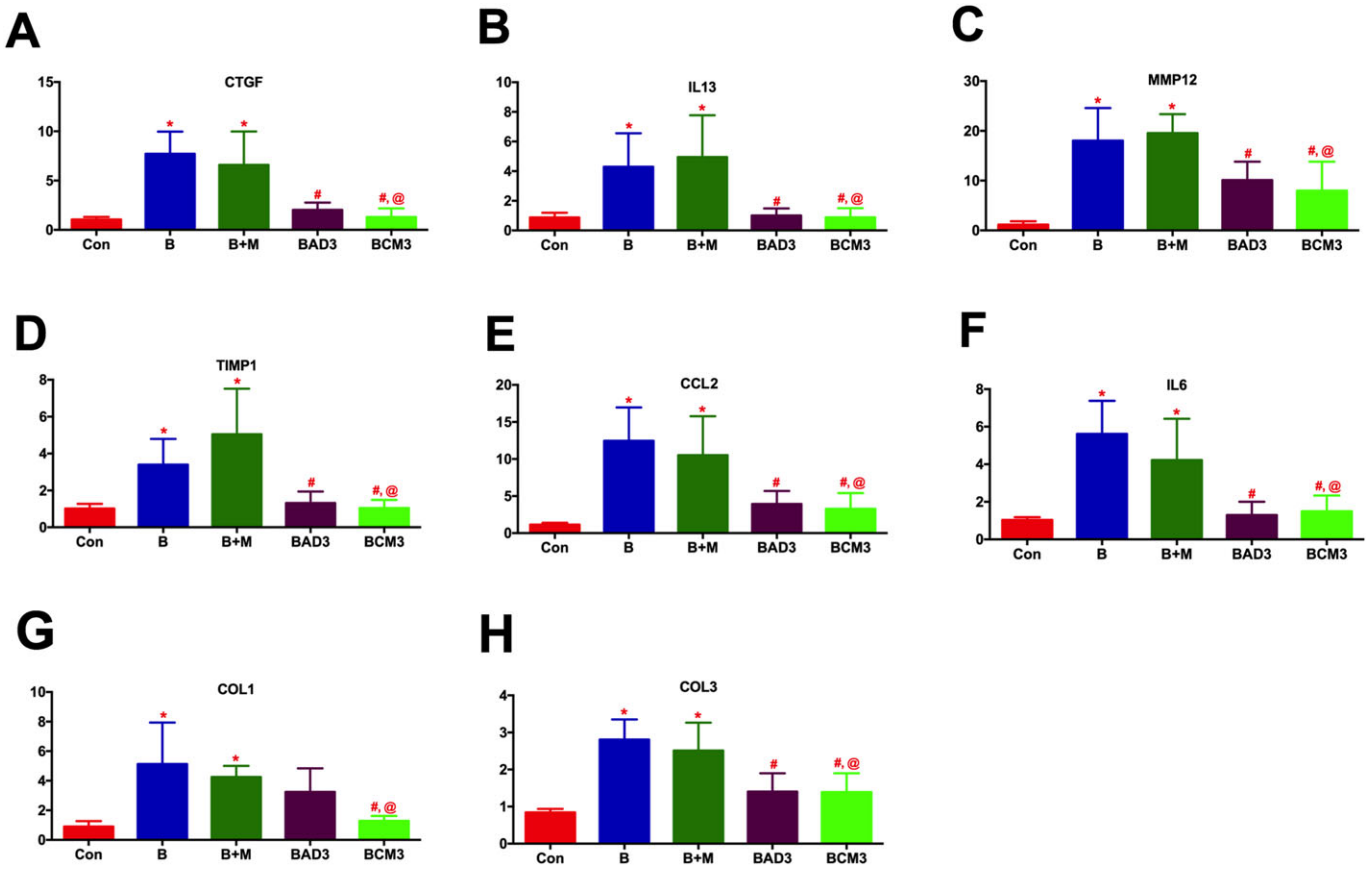

Figure 9

ASCs or CM attenuates the expression of markers of tissue remodelling and inflammation in PF (Early phase). Lung tissue harvested at the termination of the study was utilized for RT-PCR analysis: (A) CTGF, (B) IL-13, (C) MMP12, (D) TIMP1, (E) CCL2, (F) IL-6, (G) COL1, and (H) COL3. The number of animals included per group in (A)–(H) are control ($n = 5$), B ($n = 5$), B + M ($n = 4$), BAD3 ($n = 5$) and BCM3 ($n = 5$), mean ± SEM. * P value of ≤ 0.05, comparing B and B + M animals against the controls. # P value of ≤ 0.05, comparing BAD3 and BCM3 *versus* B. @ P value of ≤ 0.05, comparing BCM3 *versus* B + M.

Table 4

ASCs or CM attenuates the expression of markers of tissue remodelling and inflammation in PF (Late phase)

	Con ($n = 5$)	B ($n = 5$)	B + M ($n = 4$)	BAD7 ($n = 5$)	BCM7 ($n = 5$)
CTGF	1.12 ± 0.24	7.10 ± 1.28[a]	8.83 ± 1.65[a]	2.25 ± 0.25[b]	2.1 ± 0.25[b,c]
IL13	0.81 ± 0.09	4.68 ± 0.67[a]	5.67 ± 1.42[a]	1.01 ± 0.47[b]	1.81 ± 0.37[b,c]
MMP12	1.18 ± 0.27	34.3 ± 6.58[a]	43.83 ± 9.89[a]	10.9 ± 3.21[b]	20.46 ± 3.22[b,c]
TIMP1	1.05 ± 0.13	4.12 ± 0.81[a]	3.63 ± 0.36[a]	1.78 ± 0.33[b]	1.28 ± 0.06[b,c]
CCL2	1.12 ± 0.19	15.93 ± 3.05[a]	23.17 ± 5.65[a]	6.07 ± 0.96[b]	5.41 ± 1.32[b,c]
IL-6	0.99 ± 0.81	4.68 ± 0.50[a]	5.88 ± 0.94[a]	1.70 ± 0.19[b]	1.43 ± 0.27[b,c]
COL1	0.90 ± 0.09	5.14 ± 1.48[a]	5.95 ± 1.49[a]	4.17 ± 0.82	5.32 ± 0.91
COL3	1.13 ± 0.20	4.19 ± 1.91	2.25 ± 0.49	1.45 ± 0.21	2.30 ± 0.32

Lung tissue harvested at the termination of the study was utilized for RT-PCR analysis. Data presented are mean ± SEM, Con ($n = 5$), B ($n = 5$), B + M ($n = 4$), BAD7 ($n = 5$) and BCM7 ($n = 5$).

[a] $P \leq 0.05$, comparing B and B + M animals against the controls.

[b] $P \leq 0.05$, comparing BAD7 and BCM7 versus B.

[c] $P \leq 0.05$, comparing BCM7 versus B + M.

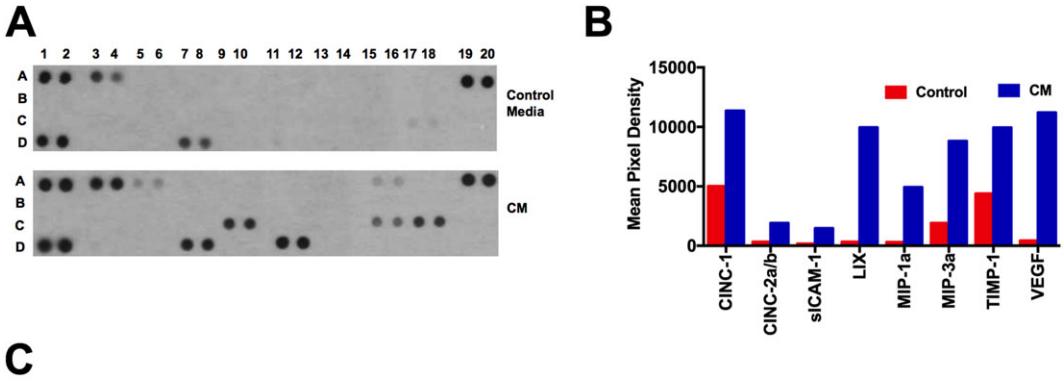

C

Coordinate	Target
A1, A2	Reference Spot
A3, A4	CINC-1
A5, A6	CINC-2α/β
A15, A16	sICAM-1
A19, A20	Reference Spot
C9, C10	LIX
C15, C16	MIP-1α
C17, C18	MIP-3α
D1, D2	Reference Spot
D7, D8	TIMP-1
D11, D12	VEGF
D17, D18	Negative Control

Figure 10

Characterization of ASCs-CM by cytokine array. In order to profile the contents of CM, we used the cytokine array system. CM, conditioned from the serum-starved ASCs were analysed for the protein contents. A total of 200 μg of protein in 285 μL were loaded in the cytokine array, and the instructions were followed as described in the kit. 285 μL of concentrated plain culture media (without serum) was used for the control array. (A) Presence of different cytokines and growth factors in control media and in CM. (B) Mean pixel density of the respective cytokines and growth factors present in CM as compared with the control media. Mean pixel density is the average of duplicates. (C) X and Y axis coordinates of cytokine array strip.

Administration of ASCs or CM in the Bleo animals completely attenuated the signals associated with inflammation and tissue remodelling. COL1 and COL3 were moderately attenuated in the early phase, although no significant change was observed in the late phase study. This lack of effect may be related to the sampling technique utilized in this study. Bleo or IPF lungs represent mixed fibrotic and non-fibrotic patches in the lungs, and thus, there is a possibility that the lung tissue chosen for the RT-PCR experiment may be a combination of both patches. However, we utilized all five-lung lobes for the estimation of hydroxyproline, and we confirmed that both ASCs and CM attenuated collagen accumulation.

Recent reports suggest that the activation of SDF-1 receptor (CXCR4 receptor) in the disease state recruits fibrocytes/inflammatory cells in addition to the stem/progenitor cells, which advances the disease (Young *et al.*, 2009; Nikam *et al.*, 2010). Inhibition of the SDF-1receptor (CXCR4) improves the lung and heart dynamics in PH (Young *et al.*, 2009; Savai *et al.*, 2012). G-CSF, which is primarily expressed at the injured site, also mobilizes the stem/progenitor cells (Weidt *et al.*, 2007). Our results suggest that ASCs or CM treatment could have either directly inhibited those cytokines or repaired the tissue injury associated with the PH lung or heart, thus minimizing the stimulus to recruit body's defence systems. The cytokine array study of the CM demonstrated the presence of chemokines and growth factors (CXCL1, ICAM-1/2, CXCL5, CCL3, CCL20, TIMP1 and VEGF), which promote chemotaxis and angiogenesis. Although chemokines are believed to participate in chemotaxis, recent studies suggest that CXCL1 (CINC-1) from ASC-CM induces neovascularization and protects the elastase induced pulmonary emphysema (Furuya *et al.*, 2012). Membrane bound ICAM activates the immune systems, while sICAM inhibits the lymphocyte function at high doses (Meyer *et al.*, 1995). Similarly, low dose CCL3/20 (MIP-1α/3α) mobilize HSCs (hematopoietic stem cells) to the inflammatory site, while its mobilization is inhibited at higher doses (Shih *et al.*, 2005). CXCL5 (LIX) and VEGF present in the CM may have a predominantly angiogenic function; however, VEGF can be anti-angiogenic too, depending on the tissue microenvironment (Voelkel and Gomez-Arroyo, 2014; D'Alessio *et al.*, 2015). Furthermore, the therapeutic benefit of VEGF in PH is controversial and still under investigation. TIMP1, present in the CM primarily inhibits tissue remodelling by blocking matrix metalloproteinase (Vieillard-Baron *et al.*, 2003). At present, it is difficult to precisely determine how the markers of inflammation, and tissue remodelling are reduced or how the CM derived chemokines/growth factors ameliorate PF or PH, since the RT-PCR experiment was performed at day 14 (PF) or 28 (PH), while ASCs or CM were administered on day 3 or 7 in PF or on day 14 in PH.

Previously, the therapeutic benefit of stem cells was believed to be mediated by their differentiation into a specific

cell-type at the injured site (Jopling *et al.*, 2011). However, recent investigations have questioned that dogma and the reparative actions are attributed to secretions of stem cells (Salgado *et al.*, 2010; Blaber *et al.*, 2012; Sabin and Kikyo, 2014). Secretions of ASCs include a wide range of bioactive molecules like cytokines, chemokines, growth factors and exosomes (Salgado *et al.*, 2010; Blaber *et al.*, 2012). Exosomes secreted by stem cells carry specific mRNA or miRNA, which could potentiate the reparative process and heal the injured tissues (Sabin and Kikyo, 2014). Interestingly, ASCs derived exosomes inhibited T cell activation, differentiation and proliferation, which emphasize the anti-inflammatory role of secretions of ASCs (Blazquez *et al.*, 2014). These reports support our findings that a single injection of CM is sufficient enough to activate the cellular regeneration or molecular signals or possibly mobilize endogenous stem/progenitor cells to salvage the injured tissue. Since ASCs do not express the major histocompatibility molecules, they can evade the host's immune surveillance and this properties make them "immune privileged" (Gonzalez-Rey *et al.*, 2010; Leto Barone *et al.*, 2013). CM could possibly evade the cell–cell contact in addition to host's immune system; therefore, making them 'super immune privileged'.

While most of the pathological symptoms observed in patients with these pulmonary diseases are observed in the MCT and Bleo animal models, angioproliferative plexiform lesion formation is an exception. However, this exception cannot be a limiting factor in defraying the therapeutic potential of ASCs or CM. To conclude, we are the first to demonstrate that either ASCs or CM treatment alone could halt the progression of MCT- or Bleo-induced PH or PF. Our studies provide the necessary information to further investigate the efficacy of cell-based secretions, yet cell-free therapy in cardiopulmonary diseases.

Acknowledgements

The authors would like to acknowledge Dr Zhi and Doug Smith for their technical assistance with Immuno fluorescence analysis.

Author contributions

A.R. designed and performed animal experiments, echocardiography, analysed data, and wrote the manuscript; V.S. performed hemodynamic measurements; E.B., A.E. and A.H. performed the histological studies; D.S. performed cytokine array experiments; A.N. and J.F. performed qPCR and analysed the data; M.K.R, supervised experiments, and provided intellectual contributions, and M.J.K supervised all experiments, analysed data and helped preparing the manuscript. All coauthors read and edited the manuscript. This work was supported by NIH R01grants, HL102033 and HL056921 awarded to M.J. K. and M.K.R. and AHA grant, SDG12080302 awarded to V.S.

Conflict of interest

The authors declare no conflicts of interest.

Declaration of transparency and scientific rigour

This Declaration acknowledges that this paper adheres to the principles for transparent reporting and scientific rigour of preclinical research recommended by funding agencies, publishers and other organisations engaged with supporting research.

References

Akhavein F, St-Michel EJ, Seifert E, Rohlicek CV (2007). Decreased left ventricular function, myocarditis, and coronary arteriolar medial thickening following monocrotaline administration in adult rats. J Appl Physiol (1985) 103: 287–295.

Alexander SPH, Kelly E, Marrion N, Peters JA, Benson HE, Faccenda E *et al.* (2015a). The Concise Guide to PHARMACOLOGY 2015/16: Overview. Br J Pharmacol 172: 5729–5143.

Alexander SPH, Davenport AP, Kelly E, Marrion N, Peters JA, Benson HE *et al.* (2015b). The Concise Guide to PHARMACOLOGY 2015/16: G protein-coupled receptors. Br J Pharmacol 172: 5744–5869.

Alexander SPH, Fabbro D, Kelly E, Marrion N, Peters JA, Benson HE *et al.* (2015c). The Concise Guide to PHARMACOLOGY 2015/16: Catalytic receptors. Br J Pharmacol 172: 5979–6023.

Alexander SPH, Fabbro D, Kelly E, Marrion N, Peters JA, Benson HE *et al.* (2015d). The Concise Guide to PHARMACOLOGY 2015/16: Enzymes. Br J Pharmacol 172: 6024–6109.

Anversa P, Perrella MA, Kourembanas S, Choi AM, Loscalzo J (2012). Regenerative pulmonary medicine: potential and promise, pitfalls and challenges. Eur J Clin Invest 42: 900–913.

Ashcroft T, Simpson JM, Timbrell V (1988). Simple method of estimating severity of pulmonary fibrosis on a numerical scale. J Clin Pathol 41: 467–470.

Bauer EM, Shapiro R, Zheng H, Ahmad F, Ishizawar D, Comhair SA *et al.* (2012). High mobility group box 1 contributes to the pathogenesis of experimental pulmonary hypertension via activation of Toll-like receptor 4. Mol Med 18: 1509–1518.

Blaber SP, Webster RA, Hill CJ, Breen EJ, Kuah D, Vesey G *et al.* (2012). Analysis of in vitro secretion profiles from adipose-derived cell populations. J Transl Med 10: 172.

Blazquez R, Sanchez-Margallo FM, de la Rosa O, Dalemans W, Alvarez V, Tarazona R *et al.* (2014). Immunomodulatory potential of human adipose mesenchymal stem cells derived exosomes on in vitro stimulated T Cells. Front Immunol 5: 556. doi:10.3389/fimmu.2014.00556.

Brunner F, Wolkart G, Haleen S (2002). Defective intracellular calcium handling in monocrotaline-induced right ventricular hypertrophy: protective effect of long-term endothelin-A receptor blockade with 2-benzo[1,3]dioxol-5-yl-3-benzyl-4-(4-methoxy-phenyl-)- 4-oxobut-2-enoate-sodium (PD 155080). J Pharmacol Exp Ther 300: 442–449.

Curtis MJ, Bond RA, Spina D, Ahluwalia A, Alexander SP, Giembycz MA *et al.* (2015). Experimental design and analysis and their reporting: new guidance for publication in BJP. Br J Pharmacol 172: 3461–3471.

D'Alessio FR, Zhong Q, Jenkins J, Moldobaeva A, Wagner EM (2015). Lung angiogenesis requires CD4(+)Forkhead homeobox protein-3(+) regulatory T cells. Am J Respir Cell Mol Biol 52: 603–610.

Dabestani A, Mahan G, Gardin JM, Takenaka K, Burn C, Allfie A *et al.* (1987). Evaluation of pulmonary artery pressure and resistance by pulsed Doppler echocardiography. Am J Cardiol 59: 662–668.

Dardalhon V, Awasthi A, Kwon H, Galileos G, Gao W, Sobel RA *et al.* (2008). IL-4 inhibits TGF-beta-induced Foxp3+ T cells and, together with TGF-beta, generates IL-9+ IL-10+ Foxp3(−) effector T cells. Nat Immunol 9: 1347–1355.

Eguchi M, Ikeda S, Kusumoto S, Sato D, Koide Y, Kawano H *et al.* (2014). Adipose-derived regenerative cell therapy inhibits the progression of monocrotaline-induced pulmonary hypertension in rats. Life Sci 118: 306–312.

Fernandez IE, Eickelberg O (2012). New cellular and molecular mechanisms of lung injury and fibrosis in idiopathic pulmonary fibrosis. Lancet 380: 680–688.

Furuya N, Takenaga M, Ohta Y, Tokura Y, Hamaguchi A, Sakamaki A *et al.* (2012). Cell therapy with adipose tissue-derived stem/stromal cells for elastase-induced pulmonary emphysema in rats. Regen Med 7: 503–512.

Gonzalez-Rey E, Gonzalez MA, Varela N, O'Valle F, Hernandez-Cortes P, Rico L *et al.* (2010). Human adipose-derived mesenchymal stem cells reduce inflammatory and T cell responses and induce regulatory T cells in vitro in rheumatoid arthritis. Ann Rheum Dis 69: 241–248.

Habiel DM, Hogaboam C (2014). Heterogeneity in fibroblast proliferation and survival in idiopathic pulmonary fibrosis. Front Pharmacol 5: 1–6.

Hameed AG, Arnold ND, Chamberlain J, Pickworth JA, Paiva C, Dawson S *et al.* (2012). Inhibition of tumor necrosis factor-related apoptosis-inducing cie (TRAIL) reverses experimental pulmonary hypertension. J Exp Med 209: 1919–1935.

Hesslinger C, Strub A, Boer R, Ulrich WR, Lehner MD, Braun C. (2012). Inhibition of inducible nitric oxide synthase in respiratory diseases. Biochem Soc Trans 37: 886–891.

Humbert M, Sitbon O, Yaici A, Montani D, O'Callaghan DS, Jais X *et al.* (2010). Survival in incident and prevalent cohorts of patients with pulmonary arterial hypertension. Eur Respir J 36: 549–555.

Ikegame Y, Yamashita K, Hayashi S, Mizuno H, Tawada M, You F *et al.* (2011). Comparison of mesenchymal stem cells from adipose tissue and bone marrow for ischemic stroke therapy. Cytotherapy 13: 675–685.

Jeon D, Chu K, Lee ST, Jung KH, Ban JJ, Park DK *et al.* (2013). Neuroprotective effect of a cell-free extract derived from human adipose stem cells in experimental stroke models. Neurobiol Dis 54: 414–420.

Jeon D, Chu K, Lee ST, Jung KH, Kang KM, Ban JJ *et al.* (2011). A cell-free extract from human adipose stem cells protects mice against epilepsy. Epilepsia 52: 1617–1626.

Jone PN, Hinzman J, Wagner BD, Ivy DD, Younoszai A (2014). Right ventricular to left ventricular diameter ratio at end-systole in evaluating outcomes in children with pulmonary hypertension. J Am Soc Echocardiogr 27: 172–178.

Jopling C, Boue S, Izpisua Belmonte JC (2011). Dedifferentiation, transdifferentiation and reprogramming: three routes to regeneration. Nat Rev Mol Cell Biol 12: 79–89.

Kanki-Horimoto S, Horimoto H, Mieno S, Kishida K, Watanabe F, Furuya E *et al.* (2006). Implantation of mesenchymal stem cells overexpressing endothelial nitric oxide synthase improves right ventricular impairments caused by pulmonary hypertension. Circulation 114: I181–I185.

Kilkenny C, Browne W, Cuthill IC, Emerson M, Altman DG (2010). Animal research: reporting in vivo experiments: the ARRIVE guidelines. Br J Pharmacol 160: 1577–1579.

Kim EH, Heo CY (2014). Current applications of adipose-derived stem cells and their future perspectives. World J Stem Cells 6: 65–68.

Lee SH, Lee EJ, Lee SY, Kim JH, Shim JJ, Shin C *et al.* (2014). The effect of adipose stem cell therapy on pulmonary fibrosis induced by repetitive intratracheal bleomycin in mice. Exp Lung Res 40: 117–125.

Leto Barone AA, Khalifian S, Lee WP, Brandacher G (2013). Immunomodulatory effects of adipose-derived stem cells: fact or fiction? Biomed Res Int 2013: 383685. http://dx.doi.org/10.1155/2013/383685.

Luo L, Lin T, Zheng S, Xie Z, Chen M, Lian G *et al.* (2015). Adipose-derived stem cells attenuate pulmonary arterial hypertension and ameliorate pulmonary arterial remodeling in monocrotaline-induced pulmonary hypertensive rats. Clin Exp Hypertens 37: 241–248.

McGrath JC, Lilley E (2015). Implementing guidelines on reporting research using animals (ARRIVE etc.): new requirements for publication in BJP. Br J Pharmacol 172: 3189–3193.

McNulty K, Janes SM (2012). Stem cells and pulmonary fibrosis: cause or cure? Proc Am Thorac Soc 9: 164–171.

Meyer DM, Dustin ML, Carron CP (1995). Characterization of intercellular adhesion molecule-1 ectodomain (sICAM-1) as an inhibitor of lymphocyte function-associated molecule-1 interaction with ICAM-1. J Immunol 155: 3578–3584.

Nemeth K, Leelahavanichkul A, Yuen PS, Mayer B, Parmelee A, Doi K *et al.* (2009). Bone marrow stromal cells attenuate sepsis via prostaglandin E(2)-dependent reprogramming of host macrophages to increase their interleukin-10 production. Nat Med 15: 42–49.

Nikam VS, Schermuly RT, Dumitrascu R, Weissmann N, Kwapiszewska G, Morrell N *et al.* (2010). Treprostinil inhibits the recruitment of bone marrow-derived circulating fibrocytes in chronic hypoxic pulmonary hypertension. Eur Respir J 36: 1302–1314.

O'Callaghan DS, Savale L, Montani D, Jais X, Sitbon O, Simonneau G *et al.* (2011). Treatment of pulmonary arterial hypertension with targeted therapies. Nat Rev Cardiol 8: 526–538.

Okano H, Nakamura M, Yoshida K, Okada Y, Tsuji O, Nori S *et al.* (2013). Steps toward safe cell therapy using induced pluripotent stem cells. Circ Res 112: 523–533.

Paul A, Srivastava S, Chen G, Shum-Tim D, Prakash S (2013). Functional assessment of adipose stem cells for xenotransplantation using myocardial infarction immunocompetent models: comparison with bone marrow stem cells. Cell Biochem Biophys 67: 263–273.

Phillips RJ, Burdick MD, Hong K, Lutz MA, Murray LA, Xue YY *et al.* (2004). Circulating fibrocytes traffic to the lungs in response to CXCL12 and mediate fibrosis. J Clin Invest 114: 438–446.

Price LC, Wort SJ, Perros F, Dorfmuller P, Huertas A, Montani D *et al.* (2012). Inflammation in pulmonary arterial hypertension. Chest 141: 210–221.

Raghu G, Collard HR, Egan JJ, Martinez FJ, Behr J, Brown KK *et al.* (2011). An official ATS/ERS/JRS/ALAT statement: idiopathic pulmonary fibrosis: evidence-based guidelines for diagnosis and management. Am J Respir Crit Care Med 183: 788–824.

Ribeiro CA, Fraga JS, Graos M, Neves NM, Reis RL, Gimble JM *et al.* (2012). The secretome of stem cells isolated from the adipose tissue and Wharton jelly acts differently on central nervous system derived cell populations. Stem Cell Res Ther 3: 18. doi:10.1186/scrt109.

Ricard N, Tu L, Le Hiress M, Huertas A, Phan C, Thuillet R *et al.* (2014). Increased pericyte coverage mediated by endothelial-derived fibroblast growth factor-2 and interleukin-6 is a source of smooth muscle-like cells in pulmonary hypertension. Circulation 129: 1586–1597.

Sabin K, Kikyo N (2014). Microvesicles as mediators of tissue regeneration. Transl Res 163: 286–295.

Sakao S, Taraseviciene-Stewart L, Wood K, Cool CD, Voelkel NF (2006). Apoptosis of pulmonary microvascular endothelial cells stimulates vascular smooth muscle cell growth. Am J Physiol Lung Cell Mol Physiol 291: L362–L368.

Salgado AJ, Reis RL, Sousa NJ, Gimble JM (2010). Adipose tissue derived stem cells secretome: soluble factors and their roles in regenerative medicine. Curr Stem Cell Res Ther 5: 103–110.

Savai R, Pullamsetti SS, Kolbe J, Bieniek E, Voswinckel R, Fink L *et al.* (2012). Immune and inflammatory cell involvement in the pathology of idiopathic pulmonary arterial hypertension. Am J Respir Crit Care Med 186: 897–908.

Schermuly RT, Ghofrani HA, Wilkins MR, Grimminger F (2011). Mechanisms of disease: pulmonary arterial hypertension. Nat Rev Cardiol 8: 443–455.

Serrano-Mollar A, Nacher M, Gay-Jordi G, Closa D, Xaubet A, Bulbena O (2007). Intratracheal transplantation of alveolar type II cells reverses bleomycin-induced lung fibrosis. Am J Respir Crit Care Med 176: 1261–1268.

Shenoy V, Ferreira AJ, Qi Y, Fraga-Silva RA, Díez-Freire C, Dooies A *et al.* (2010). The angiotensin-converting enzyme 2/angiogenesis-(1-7)/Mas axis confers cardiopulmonary protection against lung fibrosis and pulmonary hypertension. Am J Respir Crit Care Med 182: 1065–1072.

Shenoy V, Kwon KC, Rathinasabapathy A, Lin S, Jin G, Song C *et al.* (2014). Oral delivery of angiotensin-converting enzyme 2 and angiotensin-(1-7) bioencapsulated in plant cells attenuates pulmonary hypertension. Hypertension 64: 1248–1259.

Shih CH, van Eeden SF, Goto Y, Hogg JC (2005). CCL23/myeloid progenitor inhibitory factor-1 inhibits production and release of polymorphonuclear leukocytes and monocytes from the bone marrow. Exp Hematol 33: 1101–1108.

Somanna NK, Worner PM, Murthy SN, Pankey EA, Schachtele DJ, St Hilaire RC *et al.* (2014). Intratracheal administration of cyclooxygenase-1-transduced adipose tissue-derived stem cells ameliorates monocrotaline-induced pulmonary hypertension in rats. Am J Physiol Heart Circ Physiol 307: H1187–H1195.

Southan C, Sharman JL, Benson HE, Faccenda E, Pawson AJ, Alexander SP *et al.* (2016). The IUPHAR/BPS Guide to PHARMACOLOGY in 2016: towards curated quantitative interactions between 1300 protein targets and 6000 cies. Nucl Acids Res 44: D1054–D1068.

Takemiya K, Kai H, Yasukawa H, Tahara N, Kato S, Imaizumi T (2010). Mesenchymal stem cell-based prostacyclin synthase gene therapy for pulmonary hypertension rats. Basic Res Cardiol 105: 409–417.

Vieillard-Baron A, Frisdal E, Raffestin B, Baker AH, Eddahibi S, Adnot S *et al.* (2003). Inhibition of matrix metalloproteinases by lung TIMP-1 gene transfer limits monocrotaline-induced pulmonary vascular remodeling in rats. Hum Gene Ther 14: 861–869.

Voelkel NF, Gomez-Arroyo J (2014). The role of vascular endothelial growth factor in pulmonary arterial hypertension. The angiogenesis paradox. Am J Respir Cell Mol Biol 51: 474–484.

Weidt C, Niggemann B, Kasenda B, Drell TL, Zanker KS, Dittmar T (2007). Stem cell migration: a quintessential stepping stone to successful therapy. Curr Stem Cell Res Ther 2: 89–103.

Young KC, Torres E, Hatzistergos KE, Hehre D, Suguihara C, Hare JM (2009). Inhibition of the SDF-1/CXCR4 axis attenuates neonatal hypoxia-induced pulmonary hypertension. Circ Res 104: 1293–1301.

Zaiman AL, Podowski M, Medicherla S, Gordy K, Xu F, Zhen L *et al.* (2008). Role of the TGF-beta/Alk5 signaling pathway in monocrotaline-induced pulmonary hypertension. Am J Respir Crit Care Med 177: 896–905.

Zhao YD, Courtman DW, Deng Y, Kugathasan L, Zhang Q, Stewart DJ (2005). Rescue of monocrotaline-induced pulmonary arterial hypertension using bone marrow-derived endothelial-like progenitor cells: efficacy of combined cell and eNOS gene therapy in established disease. Circ Res 96: 442–450.

Zhou L, Chen Z, Vanderslice P, So SP, Ruan KH, Willerson JT *et al.* (2013). Endothelial-like progenitor cells engineered to produce prostacyclin rescue monocrotaline-induced pulmonary arterial hypertension and provide right ventricle benefits. Circulation 128: 982–994.

Supporting Information

Additional Supporting Information may be found in the online version of this article at the publisher's web-site:

http://dx.doi.org/10.1111/bph.13562

Figure S1 ASCs or CM improves the pulmonary blood flow in PH. (A) Image of pulsed Doppler recordings of all the experimental groups. After two weeks of MCT-insult, ASCs or CM was administered through the jugular vein. Pulsed Doppler recordings were measured after 28 days of MCT-insult. ASCs or CM treatment improved the pulmonary blood flow. Mid-systolic notch observed in the PH animals (white arrows) were absent in presence of ASCs or CM.

Figure S2 Dermal Fibroblasts (DF) or DF derived CM (DF-CM) did not improve MCT- induced PH. DF (1×10^6) or-DF-CM (harvested from 1×10^6 DF) were injected through-a jugular cannula, 2 weeks following the MCT insult. Following 4 weeks of MCT injection, ventricular hemodynamics were measured. (A) and (B) represent the-RVSP and RVH in MCT animals in the presence of DF or DF-CM. Data represented in (A) and (B) are mean ± SEM, Con (n = 7), MCT (n = 7), MCT + M (n = 7), MCT + DF (n = 7), MCT + DF-CM (n = 6). * Indicates a P value of ≤ 0.05, comparing MCT and MCT + M vs. control.

Figure S3 Presence of eGFP-ASCs in PH lung. In the MCT + A group, eGFP-ASCs were administered through the jugular vein after 14 days of MCT-insult. After 28 days of MCT-insult, lungs were collected, sectioned and analyzed for the presence of eGFP-ASCs by staining with GFP antibody. Images were photographed at 400×. Images represented (A) eGFP, (B) DAPI, and (C) Composite (Merge). Scale bar is 50 μm. White arrows indicate the DAPI stained eGFP-ASCs. (D) Average number of eGFP-ASCs present in 10 randomly chosen field for three different animals. Further to confirm the presence of eGFP, the same three lung samples were analyzed by real time RT-PCR. (E) Represents the C_T values of GFP and GAPDH product in RT-PCR.

Movie S1 Para-sternal short-axis ventricles view (papillary muscle level) of the control animals on Day-0.

Movie S2 Para-sternal short-axis ventricles view (papillary muscle level) of the control animals on Day-14.
Movie S3 Para-sternal short-axis ventricles view (papillary muscle level) of the MCT animals on Day-14.
Movie S4 Para-sternal short-axis ventricles view (papillary muscle level) of the control animals on Day-28.
Movie S5 Para-sternal short-axis ventricles view (papillary muscle level) of the MCT animals on Day-28.
Movie S6 Para-sternal short-axis ventricles view (papillary muscle level) of the MCT + ASCs animals on Day-28.
Movie S7 Para-sternal short-axis ventricles view (papillary muscle level) of the MCT + Media animals on Day-28.
Movie S8 Para-sternal short-axis ventricles view (papillary muscle level) view of the MCT + CM animals on Day-28.
Table S1 Rat primers used for RT-PCR experiment.